Automatic DWI infarct core segmentation in patients with acute ischemic stroke; comparison with CT-based techniques

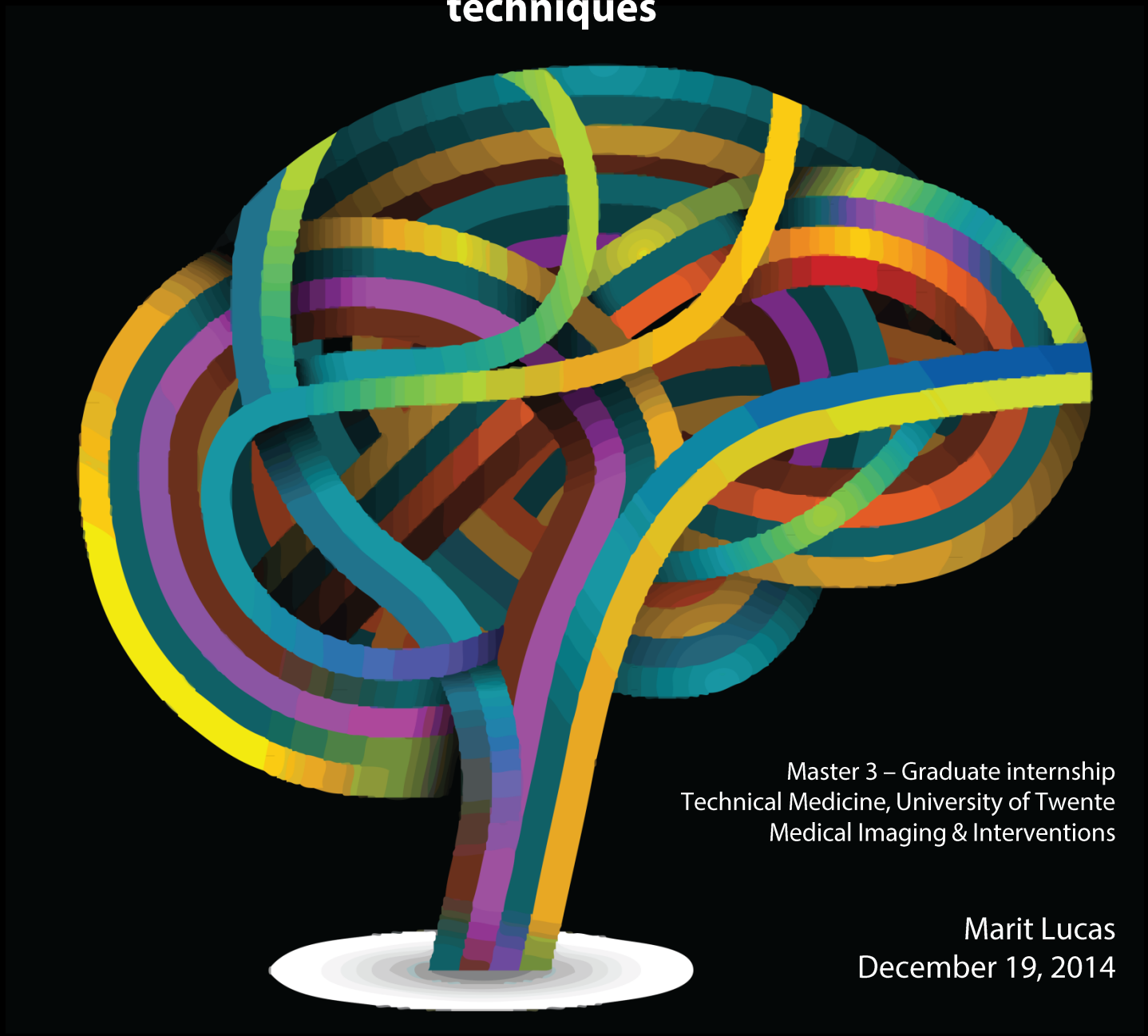

Master 3 – Graduate internship
Technical Medicine, University of Twente
Medical Imaging & Interventions

Marit Lucas
December 19, 2014

Department of Radiology
Department of Biomedical Engineering & Physics
Academic Medical Center, Amsterdam

UNIVERSITY OF TWENTE.

amc

Image adapted from the National Insitute for Clinical Application of Behaviour Science (http://www.nicabm.com/)

I Master exam committee

Prof. dr. ir. C.H. Slump [1]	Chairman & Technical Supervisor
Prof dr. C.B.L.M. Majoie [2]	Medical Supervisor
Dr. H.A. Marquering [2,3]	Technical Supervisor
Drs. A.G. Lovink [4]	Intervisor
Drs. P.A. van Katwijk [4]	Intervisor
Dr. E.J.F.M. ten Berge [4]	External member

[1] Group of Signals and Systems, University of Twente, Enschede
[2] Department of Radiology, Academical Medical Center, Amsterdam
[3] Department of Biomedical Engineering and Physics, Academical Medical Center, Amsterdam
[4] Technical Medicine, University of Twente, Enschede

II Summary

Acute ischemic stroke (AIS) is the second cause of dead worldwide, and the leading cause of acquired disability in adults. In AIS part of the brain is not sufficiently provided from blood flow due to a thrombus in the afferent vessel. All treatment options are based on the recanalization, and thus revascularization, of the occluded vessel, to restore the blood flow as soon as possible, and thus preventing the penumbra from infarction. Currently there are two main treatment options, namely (i) thrombolysis using recombinant tissue plasminogen activator intravenously (IV rtPA), which is proven to be beneficial within 4.5 hours after symptom onset and (ii) intra-arterial treatment (IAT), in which the thrombus can be mechanically removed from the vessel. Recently, it is proven that IAT within 6 hours after symptom onset is effective as an addition to the normal intravenous treatment. A drawback of IAT is the higher risk of hemorrhage, certainly in large infarct cores, and thus better selection of patients, can further improve the efficiently of the IAT.

Currently, treatment decisions are mainly based on the time expired since the time of onset. However, the time of onset is not always clear, e.g. in wake-up strokes. In addition, it is known that even after 12 to 24 hour after symptom onset viable penumbra can still be present. For these reasons, clinical decision making based on time alone is unlikely to provide the best selection criterion. Infarct core volume might be more predictive, as a large volume of the infarct core is associated with poor collateral flow. It is known that the quality of the collateral flow is strongly associated with infarct growth.

Diffusion weighted MR imaging (MR-DWI), and its derivate apparent diffusion coefficient (ADC) image, is assumed to be the reliable golden standard in determining the infarct core volume within the first minutes after ictus. However, this MR imaging is uncommon in Dutch emergency departments (ED). Perfusion CT (CTP) is increasingly used as a diagnostic tool for patients suffering from acute ischemic stroke. It can be rapidly performed in almost every patient, and claims to be able to make a distinction between the infarct core and the salvageable penumbra.

Segmentation of the infarct core on CTP using the commercially available Philips workstation can give a false positive core (meaning that this part of the CTP core is not in the final infarct region) up to 60% of the CTP infarct core. This implies that the current segmentation of the infarct core on CTP is not optimal and raises the question whether it is possible to optimize the CTP data analysis based on the segmented ADC infarct core, using analysis of the absolute and relative parameter values found in the infarct core, as well as applying a combination of thresholds using voxel-based machine learning.

In the first chapter of this thesis, I give a general introduction in the ischemic stroke, and its treatment options. I also discuss the importance of using infarct core volume for selection of the patients.

In the second chapter, the two imaging techniques for determining the infarct core volumes are explained, namely diffusion weighted MR imaging (MR-DWI) and CT perfusion (CTP). Also the state-of-the-art post-processing of CTP is discussed, i.e. filtering and deconvolution techniques.

Afterwards, three separate chapters about the segmentation of the infarct core will follow. The first of these chapters is about the automatic segmentation of the infarct core on MR-DWI. Afterwards, a comparison with follow-up imaging must reveal whether this segmentation is reliable. A relation is expected between the severity of the diffusion restriction and the acute infarct core volume.

Automatic segmentation of the infarct core on ADC images is possible using a threshold of 600×10^{-6} mm^2/s in combination with morphological operations. The median value of the diffusion restriction is associated with the infarct core size. Qualitative assessment of the ADC infarct core with the follow-up CT suggests no reversal of the ADC infarct core.

Afterwards, a chapter about the results of the state-the- of-art post-processing of the CTP will follow. Post-processing of the raw data, by implementing motion correction and TIPS bilateral filtering, is likely to improve the outcomes of PMA. Afterwards, a comparison of the parameter maps obtained by various deconvolutions options, as offered by PMA, is done. Large differences between the different deconvolutions are observed, mainly in the MTT and the Tmax parameter maps.

The last chapter concerns the analysis of CTP data based on the segmented MR-DWI infarct cores, using analysis of the absolute and relative parameter values found in the infarct core, while differentiation between gray and white matter. Applying a combination of thresholds using voxel-based machine learning is also pursued to get a better insight in the important thresholds for the segmentation of the infarct core.

Large overlap between the parameter values found in healthy and core tissue is observed. Differentiation between white and gray matter is essential in future research, as significant differences were found in the parameters for these tissues. Comparison with the contralateral side is most promising based on various classification trees.

III Abbreviations

ADC	Apparent diffusion coefficient
AIS	Acute ischemic stroke
AT	Arrival time
bSVD	Block-circulant SVD
CBF	Cerebral blood flow
CBV	Cerebral blood volume
CT	Computed tomography
CTP	CT perfusion
dSVD	Delay SVD
DWI	Diffusion weigthed imaging
GM	Gray matter
IAT	Intra-arterial treatment
IV	Intravenous
MR CLEAN	Multicenter Randomized Clinical trial of Endovascular treatment for Acute ischemic stroke in the Netherlands
MTT	Mean transit time
NCCT	Non-contrast CT
PMA	Perfusion Mismatch Analyzer
PWI	Perfusion weighted imaging
rtPA	Recombinant tissue plasminogen activator
sSVD	Standard SVD
SVD	Singular value decomposition
TIPS	Time-intensity profile similarity
WM	White matter

Table of Contents

1. Introduction

Stroke is the second most common cause of death worldwide [1], with an incidence between 101.2 to 239.3 per 100.000 males in Europe. The incidence in women is lower, ranging from 63.0 to 158.7 per 100.000 females [2]. The number of strokes in Europe is likely to increase towards 1.5 million in 2030 due to demographic changes [1,3]. Furthermore, stroke is the leading cause of acquired disability in adults (i.e. dementia (22.5%), institutionalization (15%)) [4]. A stroke is characterized by a rapid loss of brain functions due to a disturbance of blood supply of the brain. A distinction can be made between (i) ischemic stroke, observed in 87% of the cases and (ii) hemorrhagic strokes, accounting for 13% of the strokes [5]. This research focuses on the ischemic stroke, in which a cerebral artery is occluded by an embolus, such as a thrombus. This disturbs the blood flow and leads to termination of neural activity within seconds, and deterioration of the energy state and ion homeostasis of cells within minutes [1,6].

In ischemic stroke, the brain tissue can be differentiated in different levels of ischemia. The ischemic core, suffering from hypoxic cell death (infarction), is irreversible damaged tissue. Surrounding the ischemic core is a region of functionally impaired, but structurally intact tissue, which is called the ischemic penumbra. This region is at risk of infarction, and may benefit from fast revascularization, and is for this reason assumed to be the salvageable tissue [1]. The region surrounding the penumbra is called the benign oligaemia, in which reduced blood flow is observed, however, brain functions are not affected [7,8].

1.1 Treatment of acute ischemic stroke

The default treatment of acute ischemic stroke is administration of recombinant tissue plasminogen activator intravenously (IV rtPA), which is proven to be beneficial within 4.5 hours after symptom onset [9]. In the United States, less than 10% of the patients with ischemic stroke met the eligibility criteria for intravenous thrombolysis because of an unknown time of symptom onset and long traveling times in rural areas [10]. After this time-frame of 4.5 hours, intra-arterial thrombolysis has been suggested to be beneficial until six hours after symptom onset [5]. In intra-arterial thrombolysis a lower dose of thrombolytic agent is administered close to the thrombus. Due to the lower dose, this treatment is associated with a lower risk of hemorrhage [11]. Intra-arterial thrombectomy, in which the thrombus is removed mechanically, is assumed to be beneficial until eight hours after symptom onset [5]. However, the risks of intra-arterial treatment are not insignificant. In 5-7% of the cases, a clinically significant complication is associated with the treatment, and in 6 to 15% of the cases the treatment induces a symptomatic intracranial hemorrhage [12]. Other complications of intra-arterial treatment is damaging the arterial wall and fragmentation (and embolization) of the thrombus. Furthermore, intra-arterial therapy requires more preparation time than intravenous therapy due to the mobilization of the interventional team [10].

Intra-arterial treatment (IAT) in large vessel occlusion is currently the subject of many studies. There are multiple instruments designed for mechanical revascularization of large vessels. Multiple researchers have compared the different instruments. Stent retrievers obtain the highest rate of recanalization. However, improved reperfusion due to recanalization is not a guarantee for clinical efficacy [10,13].

Recent developments in treatment

Multiple randomized clinical trials studied the advantage of intra-arterial treatment in addition to regular intravenous treatment. In the Netherlands, a large multicenter study has been set up; Multicenter Randomized Clinical trial of Endovascular treatment for Acute ischemic stroke in the Netherlands (MR CLEAN), in which the safety and efficacy of intra-arterial treatment is examined. In this study, most of the endovascular treatments are conducted using stent-retrievers. In contrast to the other studies published [10,14,15], the beneficial effect of IAT in stroke patients is proven in the MR CLEAN trial [16]. The absence of a more beneficial outcome for patients treated with intra-arterial treatment in the other researches can probably be elucidated by multiple explanations. For instance, in the Interventional Management of Stroke (IMS) and MR RESCUE studies, most patients were treated with the MERCI retriever. This retriever is associated with lower percentages of reperfusion compared with a stent retriever, and therefore associated with a less favorable

outcome [10,13,14]. Another explanation could be that in other studies, the presence of thrombus was not always proven using CTA.

Nowadays, multiple studies have tried to select patients with a relatively large penumbra, penumbral pattern or PWI-DWI mismatch (meaning volume of the penumbra ≥120% of the ischemic core volume), which are likely to benefit most from intra-arterial treatment. It is known that there is a linear relationship between the quality of collaterals and penumbra loss per hour [17]. Imaging of the infarct core can be performed using diffusion weighted images (DWI), while the penumbra can be visualized using perfusion weighted images (PWI) [10,18]. In the DEFUSE trial, the effect of intra-arterial treatment in patients with a PWI-DWI mismatch was compared with patients without mismatch. In this trial, the group with a PWI-DWI mismatch had a (non-significant) more favorable outcome when reperfusion was achieved [15]. The effect of treatment might also be influenced by the time between IV rtPA and IAT, as the patients without mismatch generally received the treatment sooner, which is beneficial for clinical outcome [15]. The MR RESCUE study examined whether patients with a favorable penumbral pattern had a better outcome than patients without this favorable pattern. In this case, the favorable penumbral pattern was defined as a small core with a large penumbra or, more exactly, by an infarct core ≤90ml and the infarct core ≤70% of the total at risk tissue for infarction (ischemic core and penumbra together). They concluded that patients with a favorable penumbral pattern have better outcomes than patients without [14].

To reduce the number of futile intra-arterial therapies, patients that are more likely to benefit from intra-arterial treatment must be selected. The reason for this selection is twofold, firstly, the treatment has a high chance of complications, certainly in large infarct core volumes [10,12,19]. Secondly, because the treatment is expensive, reduction of the number of futile intra-arterial treatments is beneficial economically.

Currently, in some studies a PWI-DWI mismatch of >20% is used as a criterion for the selection of patients for intra-arterial treatment [17,20,21]. This selection criterion is assumed to have too little discriminatory power, as in most patients with a large vessel occlusion, the mismatch is more than 20% [21]. This suggests that the addition of PWI is not necessary. In a study of Yoo *et al.* [21], similar rates of favorable outcomes were obtained by a selection based on DWI infarct core volumes only. This supports the hypothesis that there exists a threshold for core volume (based on DWI) in which patients benefit from endovascular treatment. In multiple studies, the threshold is set around 70 cm^3 [8,10]. The patients with large infarct cores (>70 cm^3) have the highest chance on symptomatic intra-cerebral hemorrhage [19], and have the worst pial collateral flow [22]; another factor associated with unfavorable clinical outcome [21]. Morais et *al*. concluded that currently, the most reliable measures for intra-arterial treatment decision-making is the ASPECTS score on non-contrast computed tomography (NCCT) and the core volume at DWI [23].

In 2000, the Alberta Stroke Program Early CT score (ASPECTS) was introduced to systematically analyze the territory of the Middle Cerebral Artery (MCA) for early ischemic changes (EIC) [24]. ASPECTS score is based on the subtle changes that can be seen on NCCT. These subtle changes are the result of edema in the regions of infarctions [6]. As these changes are subtle on NCCT, a large variation in inter-observer agreement is observed in multiple studies. Wardlaw *et al*. examined multiple studies on the detection of EIC on NCCT with an intraclass correlation coefficient, κ ranging from 0.14-0.78 [25].

DWI is the most sensitive and specific method to visualize the infarct core volume in the acute setting [26]. However, quantitative measures on DWI images are not possible, as the DWI signal strength depends, among others, on the magnetic field strength [27]. This field is commonly inhomogeneous in MR scanners. For this reason the apparent diffusion coefficient (calculated from six DWI series) is used for quantified measurements. Manual outlining of volumes on DWI is associated with larger intra- and inter-observer variability, in comparison with ADC outlining [28]. Furthermore, manual delineation is time demanding, resulting in a potential prolongation of the period before clinical decision making, which is disadvantageous for clinical outcome. For this reason a fast and automatic method is desired to determine the DWI infarct core volume. A recently published automatic technique in which the penumbra was segmented on ADC value, can select a volume based on thresholding with a sensitivity of approximately 70%, and a specificity around 80% [29]. In other recent studies, accuracies of this technique ranged between

50-70% [30,31]. However, better results are obtained using the Rapid processing of PerfusIon and Diffusion (RAPID) method [18]. This method was designed in 2010 to automatically calculate the infarct core and penumbra and was used for mismatch analysis in the DEFUSE II trial. With this method, the largest deviation between manual outlining and the automatic technique of the infarct core was approximately 10 mL. However, the standard deviation of the difference in volume was just 2.5 mL [18].

In some studies, (automatic) outlining of the infarct core based on DWI is used for treatment decision making. Nevertheless, the clinical application of MRI has been restricted in emergency departments, as the availability of scanners is limited and not all patients are eligible for MRI scanning due to metal implants. CT on the other hand, has a much wider availability in emergency departments, and nowadays most multi-slice CT scanners are able to generate CT perfusion (CTP) images [32]. Research to define CT perfusion thresholds and parameters that best matches the infarct core on MR DWI is ongoing [32–35]. A major limitation in these studies is the time allowed between CTP and MR DWI acquisitions, which varies between less than 1 hour [32,33] to 24 hours [35]. The study of Campbell *et al.* [33], with the smallest interval between CTP and MR acquisition, revealed that a threshold of 31% of the cerebral blood flow (CBF), in comparison with the contralateral side, gives the best estimation of the ischemic core. However, a mean overestimation of 11mL was observed, and the Bland-Altman 95% limits of agreement were -46.9 to 24.2 mL [33]. These regions of overestimation were mostly present in the white matter. These volume differences can be explained by several reasons, (i) reduction in CBF in the regions of leukoaraiosis, (ii) the relatively low contrast-to-noise ratio of CTP compared with MRI, and (iii) the physiological difference in CBF between gray and white matter [30,31,33,36], which is not considered in CTP analysis techniques. Campbell *et al.* also assumed that based on infarct core segmentation on CBF maps, the physician was able to make the treatment decision for the majority of the patients, without requiring a MR DWI [33]. However, it is known that the appropriate thresholds are dependent on the software package used, and for this reason not universally usable [35]. Even when the same source data was used, the commercial software resulted in significantly different CT perfusion imaging maps [37].

1.2 Objective

Patient selection based on infarct core volume is probably the most promising technique for clinical treatment decision making. Infarct core volume can be segmented on apparent diffusion coefficient images, however MR imaging is uncommon in Dutch emergency departments (ED).

The main objective of this research is to improve the (automatic) segmentation of the infarct core on both DWI as CTP images. To achieve this, three objectives are stated.

1) Implement a method to automatically segment the infarct core on ADC images, based on Straka *et al.* [18]
2) Improvement of the post-processing of CTP source data, using motion correction and TIPS bilateral filtering, as well as obtaining the different parameter maps.
3) Evaluation of the parameter maps of the CTP, at the location of the ADC infarct core , to improve the segmentation of the infarct core on CTP.

2. Technical context

Imaging of the infarct core in an acute setting is nowadays mostly done using diffusion weighted MR imaging and CT perfusion. In this chapter, a description of those two techniques is given, as well as a brief overview of some of the state-of-the-art post-processing options to obtain the infarct cores.

2.1 Diffusion weighted imaging

Magnetic resonance (MR) diffusion weighted imaging (DWI) visualizes diffusion and is commonly used for imaging of the brain. Diffusion is the random movement of (in this case water molecules, H_2O) within tissues [27,38–40]. In case of free diffusion, the displacement is isotropic. However, biological tissues are highly heterogeneous medias that consist of various compartments and barriers of different diffusivities [39]. DWI uses a spin echo pulse sequence, in which the first pulse (G_{diff}) dephases the magnetization of moving and static spins. The second pulse only rephases the static spins 100% (as these have not moved), while the moving spins do not (completely) rephase. Practically this means that in areas of slow diffusion, there is less signal damping (bright) than in regions with fast diffusion (dark). The contrast can be adjusted by changing the b-value, meaning that higher b-values will result in stronger attenuation of free water. This value is dependent on the amplitude of the diffusion gradient pulses (G), the duration of the pulses (δ), the duration between pulses (Δ) and the gyromagnetic ratio (for H_1 42.576 MHz/T). The b value is given by [38]:

$$b = \gamma^2 G^2 \delta^2 \left(\Delta - \frac{\delta}{3}\right) \tag{2.1}$$

As the diffusion of water is possible in all directions, DWI images are made in all spatial directions (x, y and z)

However, quantitative measures on DWI images are not possible, as the DWI signal strength is dependent on the magnetic field strength. This field is assumed to be inhomogeneous in MR scanners, and for this reason the apparent diffusion coefficient is used for quantified measurements (see Section 2.1.1).

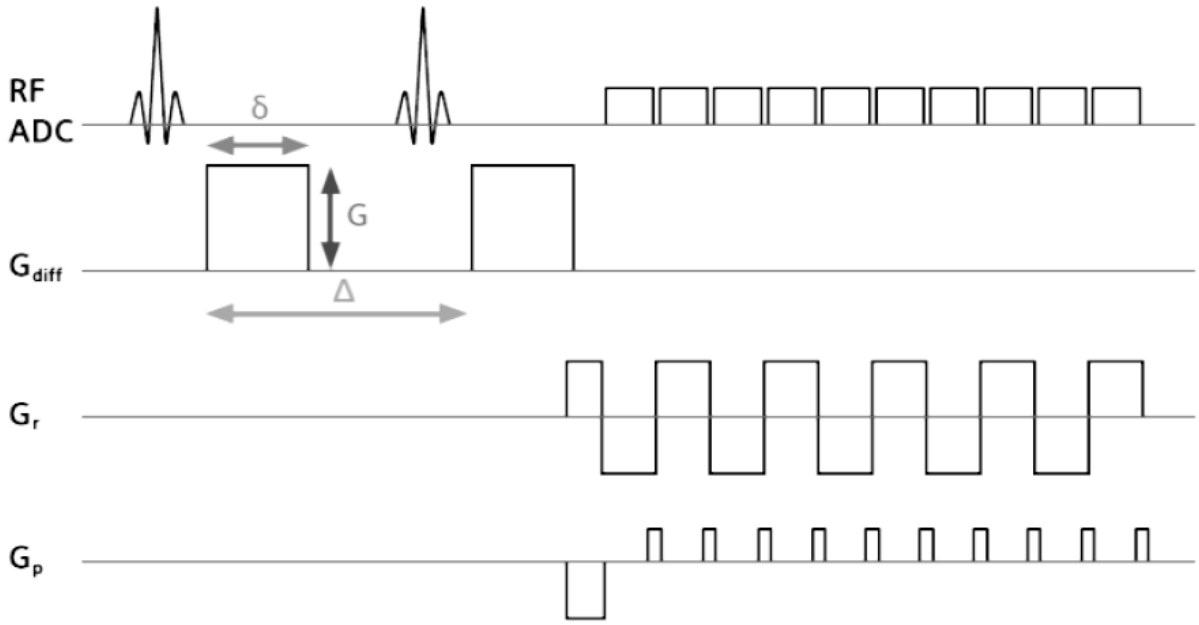

Fig 2.1 Acquisition of DWI, in which the G_{diff} is needed to dephases and rephrases the static spins. The duration of these pulses, as well as the time between the pulses and amplitude influences the b-value, also associated with the weighting of the diffusion.

2.1.1 Apparent diffusion coefficient

When DWI images are made for different b-values, the apparent diffusion coefficient (ADC) can be calculated. Normally for acute ischemic stroke imaging, DWI images are made with b=1000 and b=0 (no diffusion contrast) [15,17,18,27,29,41]. This value follows from [18]:

$$ADC = -\frac{1}{b} \ln \left(\frac{S_b = 1000}{S_b = 0} \right) \quad (2.2)$$

Ischemic tissue is recognizable by the low diffusion, as that part of the brain tissue is separated from the 'healthy' perfused brain.

2.2 Non-contrast computed tomography

Non-contrast CT (NCCT) is often used in the differentiation of acute ischemic from hemorrhagic stroke. As blood is clearly visible on NCCT images, this scan is used to rule out hemorrhagic strokes. To systematically analyze the territory of the Middle Cerebral Artery (MCA) for early ischemic changes (EIC), the Alberta Stroke Program Early CT score (ASPECTS) was introduced in 2000 [24]. These early ischemic changes are the result of the increase in edema, leading to a slight hypodensity compared with the 'healthy' contralateral side.

2.3 Perfusion computed tomography

Perfusion computed tomography (CTP) is currently the most frequently applied technique to image the size of the infarct core and the assumed penumbra. In CTP, contrast agent is injected, and soon after the injection, the brain is scanned several times in a short interval, i.e. twenty-five times during 48 seconds. These images contain the inflow and (part of the) outflow of the contrast agent, and are therefore a measure of the perfusion. Based on the tissue curves, several maps of the brain can be made for different parameter values. The most important ones are the cerebral blood volume (CBV) and mean transit time (MTT) of the contrast agent. The cerebral blood flow (CBF) is obtained by dividing these parameters.

2.3.1 Calculation of CTP parameters

The technique to calculate the different perfusion parameters can be seen in Fig 2.2. Based on the tissue attenuation curve, i.e. the change in intensity in each voxel over time, an estimation of the blood volume, flow and transit time can be made. A drawback of this technique is that it is prone to noise in the tissue curve. Therefore, various alternatives to obtain the parameter maps more robustly have been introduced. Both model dependent and model independent approaches for deconvolution have been introduced. These are introduced below.

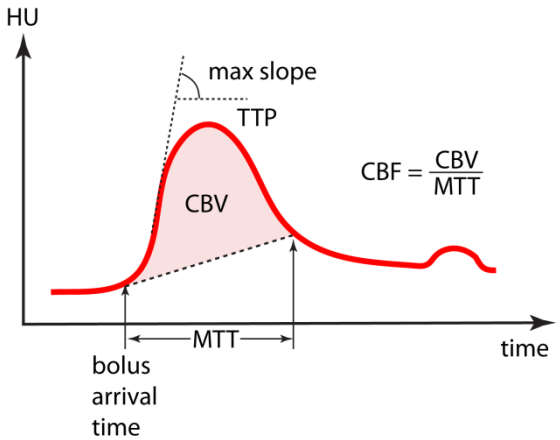

Fig 2.2 Technique for determination of the CBV, CBF, MTT and Tmax for a tissue curve.

Model independent

Nowadays the most common technique to calculate the parameter maps is using singular value decomposition (SVD). This approach uses the tissue attenuation curves ($C_{tissue}(t)$) and the arterial input function (AIF(t)) obtained from several selected voxels in the artery, to obtain the residue function (R(t)), which is the real tissue response of the specific voxel. The residue function is obtained via the following transformation:

$$\Delta t \begin{pmatrix} AIF(t_1) & 0 & \cdots & 0 \\ AIF(t_2) & AIF(t_1) & \cdots & 0 \\ \cdots & \cdots & \cdots & 0 \\ AIF(t_N) & AIF(t_{N-1}) & \cdots & AIF(t_1) \end{pmatrix} \cdot \begin{pmatrix} R(t_1) \\ R(t_2) \\ \cdots \\ R(t_N) \end{pmatrix} = \begin{pmatrix} C_{tissue}(t_1) \\ C_{tissue}(t_2) \\ \cdots \\ C_{tissue}(t_N) \end{pmatrix} \quad (2.3)$$

Equation 2.3 represents a standard single value decomposition (sSVD)[42,43].

Despite the more robust way of calculating the parameter maps, large errors can emerge using this technique. For instance, when the arterial input function (AIF) is delayed, e.g. by selecting a truncated artery, the contrast in the tissue can arrive sooner than in the artery. This results in an incorrect residue function (R(t)). To avoid any faulty residue functions, and therefore incorrect maps, a delay insensitive SVD can be used. The most commonly used delay insensitive singular value decomposition technique used is the block-circulant SVD. In this case the arterial input function is replaced by:[44]

$$AIF'(t) = AIF(t - t_d), \quad (2.4)$$

And the residue function (R(t)) is replaced by:

$$R'(t) = R(t + t_d). \quad (2.5)$$

Other delay insensitive SVD techniques are abbreviated as dSVD, in which the delay in contrast agent arrival, between the AIF and tissue curve, is corrected. This can be done using the bolus arrival time (AT) of the tissue curve, a clear definition is an increase of 5% of the peak value of the tissue curve. In this case

$$AIF'(t) = AIF(t + t_d), \quad (2.6)$$

The cerebral blood volume is given by the area under the tissue curve of the volume of interest (C_{VOI}) divided by the area under the venous output function (C_v), or in mathematical form by

$$CBV = \frac{\kappa}{\rho} \cdot \frac{\int_{-\infty}^{\infty} C_{VOI}(\tau)d\tau}{\int_{-\infty}^{\infty} C_v(\tau)d\tau}, \quad (2.7)$$

where κ corrects for the hematocrit (HCT) difference between small vessels (HCT_{SV}=0.25) and large vessels (HCT_{LV}=0.45) using the formula $\kappa = \frac{(1-HCT_{LV})}{(1-HCT_{SV})} \approx 0.007$. ρ is the brain tissue density (1.04 g/mL). After the calculation of the CBV using Equation 2.7 and the CBF based on the maximum R(t), the MTT is given by dividing the CBV map by the CBF map [45].

Model dependent

In 2012, Boutelier *et al.* [46] introduced a novel method to calculate the parameter maps using Bayesian hemodynamic parameter estimation. This method is nowadays used in the commercially available Olea Medical software. For this estimation, the AIF is supposed to be known. This software estimates the blood flow CBF, residue function R(t) and delay t_d. The set of these parameters is called Θ, while θ is a single parameter, i.e. blood flow. Using the following Bayes rule

$$P(\Theta|D) = \frac{p(\Theta)p(D|\Theta)}{\int_\Theta p(\theta)p(D|\Theta)d\theta}$$

In which p(Θ) is the joint prior probability and p(D|Θ) the likelihood. Using likelihood and joint prior probability distributions, the posterior probability (P(Θ|D)) can be calculated for these three parameters. Afterwards, marginal posterior distributions using the Bayes estimators can calculate the probability of a single parameter using

$$P(\theta|D) = \int_{\Theta\backslash\theta} P(\theta|D)d(\Theta\backslash\theta)$$

In which is Θ\θ is the complement of parameter θ in the set of all parameters Θ. The evaluation of the posteriors and estimators involves the calculation of high-dimensional multiple definite integrals. If the blood flow, delay and residue function is known, calculation of the time attenuation curves, and therefore the CBV and MTT, is possible. The largest advantage is the robustness of this method, especially when noise

levels are high [47,48]. This method mainly improves the measurements of blood flow (CBF) and mean transit time (MTT). It is known that the CBF can be underestimated in regions of high flow when using a SVD. The MTT can be negative or extremely low in regions of hypoperfusion using a SVD, while the opposite is expected. The estimation of the cerebral blood volume (CBV) is on the other hand slightly less accurate as compared to SVD techniques. Another drawback is this Bayesian method is that the Tmax is only dependent on delay t_d, while in SVD this is a combination of delay and MTT [48].

2.3.2 Noise reduction of CTP data

The main drawback for using X-rays for imaging is the risk of inducing tissue damage due to its carcinogenic effects. Especially in the technique of CTP, where a certain volume of the brain is imaged often over time, the radiation dose accumulates to a large amount. For this reason, a tradeoff between radiation dose and image quality (contrast to noise ratio – CNR) is made.

Reducing the effects of noise is of major importance in CTP analysis. It is know that the quality of the parameter maps is largely influenced by the noise of the raw data[49]. Nowadays, various techniques are used to reduce the noise in the spatial domain. There are plenty of implementations of the 2D and 3D Gaussian filter[50,51] and of wavelet and curvelet transforms. However, these filters do not take the fourth dimension of CTP images, e.g. time, into account. For this reason, Kosior investigated the use of 4D filters in the filtering of perfusion data[52]. In their study, a comparison between a 4D Gaussian and a 4D bilateral filter was made. The largest advantage of the bilateral filter was that besides the smoothing, edges remained sharp. The largest drawback of using 4D bilateral filtering is that it is computational demanding, which may result in delays in clinical decision making.

In 2009, Mendrik *et al*. suggested a bilateral filtering method using the time-intensity profile similarity (TIPS) [53]. This method has two main advantages, (i) the time intensity profiles are preserved, and (ii) it is much faster than the 4D bilateral filtering as a result of using a 3D kernel instead of a 4D kernel.

2.3.2.1 TIPS filter

In bilateral filtering, each voxel value in the image is replaced by a weighted average of similar and nearby voxel values. The Gaussian closeness $c(\xi, \boldsymbol{x})$ function is given by [54]

$$c(\xi, \boldsymbol{x}) = \exp\left(-\frac{1}{2}\left(\frac{d(\xi, \boldsymbol{x})}{\sigma_d}\right)^2\right), \tag{2.8}$$

Where $d(\xi, \boldsymbol{x})$is the Euclidean distance between voxel **x** and its neighbour ξ, and the standard deviation (σ_d) determines which distance is considered to be close. The pixel similarity function $s(\xi, \boldsymbol{x})$ is defined as [54]

$$s(\xi, \boldsymbol{x}) = \exp\left(-\frac{1}{2}\left(\frac{\delta(\boldsymbol{f}(\xi), \boldsymbol{f}(\boldsymbol{x}))}{\sigma_r}\right)^2\right), \tag{2.9}$$

In which $\delta(\boldsymbol{f}(\xi), \boldsymbol{f}(\boldsymbol{x}))$ is the absolute intensity difference between the voxels **x** and ξ. The intensities are assumed to be similar when their absolute difference is smaller than the standard deviation (σ_r) of the Gaussian function. Where the TIPS filter differs from the bilateral filter is that it uses a time-intensity profile similarity (TIPS) function instead of a conventional absolute intensity difference similarity function ($s(\xi, \boldsymbol{x})$). The TIPS function ($p(\xi, \boldsymbol{x})$) is given by [53]

$$p(\xi, \boldsymbol{x}) = \exp\left(-\frac{1}{2}\left(\frac{\zeta(\xi, \boldsymbol{x})}{\sigma_\zeta}\right)^2\right), \tag{2.10}$$

Where $\zeta(\xi, \boldsymbol{x})$ is the sum of squared differences (SSD) and is a measure for the time-intensity profile at voxel **x** and that at neighboring voxel ξ. The standard deviation $\sigma_\zeta$determines up to which SSD measure the time-intensity profiles are considered to be similar. This parameter (σ_ζ) can be calculated from an area of the

image where the intensity is assumed to be identical over time. This can be for instance the cerebrospinal fluid in ventricles in the brain or the air outside the skull. The SSD is given by

$$\zeta(\xi, \boldsymbol{x}) = \frac{1}{T}\sum_{t=0}^{T=1}\Big(I\big(\xi(x,y,z,t)\big) - I\big(\boldsymbol{x}(x,y,z,t)\big)\Big)^2 \tag{2.11}$$

where the intensity of voxel **x** is subtracted from the intensity of neighboring voxel ξ for the whole temporal domain. T is the size of the temporal domain.

Combining all these measures, yields the bilateral filtering equation

$$\boldsymbol{h}\big(\boldsymbol{x}(x,y,z,t)\big) = \frac{1}{n(\boldsymbol{x})}\sum_{i=-m}^{m}\sum_{j=-n}^{n}\sum_{k=-o}^{o} I\big(\xi(x+i, y+j, z+k, t)\big)\, c(\xi, \boldsymbol{x}) p(\xi, \boldsymbol{x}) d\xi \tag{2.12}$$

Where m, n and o are half of the kernel sizes in respectively x,y and z direction, $c(\xi, \boldsymbol{x})$ is the Gaussian closeness function (Eq. 2.8) and $p(\xi, \boldsymbol{x})$ the TIPS function (Eq 2.10). The normalization is done by n(**x**) using the following formula

$$n(\boldsymbol{x}) = \sum_{i=-m}^{m}\sum_{j=-n}^{n}\sum_{k=-o}^{o} c(\xi, \boldsymbol{x}) p(\xi, \boldsymbol{x}) d\xi \tag{2.13}$$

3. Acute infarct core segmentation on diffusion weighted imaging

Acute ischemic stroke (AIS) is the second cause of dead worldwide, and the leading cause of acquired disability in adults [1,4]. In AIS part of the brain is not sufficiently provided from blood flow due to a thrombus in the afferent vessel. All treatment options are based on the recanalization, and thus revascularization, of the occluded vessel, to restore the blood flow as soon as possible, and thus preventing the penumbra from infarction. Currently there are two main treatment options, namely (i) thrombolysis using recombinant tissue plasminogen activator intravenously (IV rtPA), which is proven to be beneficial within 4.5 hours after symptom onset [9] and (ii) intra-arterial treatment (IAT), in which the thrombus can be mechanically removed from the vessel. Recently, it is proven that IAT within 6 hours after symptom onset is effective as an addition to the normal intravenous treatment [16]. A drawback of IAT is the higher risk of hemorrhage, certainly in large infarct cores [10,12,19], and thus better selection of patients, can further improve the efficiently of the IAT.

Currently, treatment decisions are mainly based on the time expired since the time of onset. However, the time of onset is not always clear, e.g. in wake-up strokes. In addition, it is known that even after 12 to 24 hour after symptom onset viable penumbra can still be present. For these reasons, clinical decision making based on time alone is unlikely to provide the best selection criterion. Infarct core volume might be more predictive, as a large volume of the infarct core is associated with poor collateral flow [22,23]. It is known that the quality of the collateral flow is strongly associated with infarct growth [55,56]. Moreover, hemorrhages are more common in large infarct cores, and for this reason the selection based on infarct core volume might be twofold. In (i) patients with a good collateral flow, and therefore small infarct core outside the 6 hour treatment window, a treatment might be still beneficial, and (ii) in a patient with a poor collateral flow, and thus large infarct core, a better assessment can be made of the pros and cons, e.g. hemorrhage, of the IAT.

Diffusion weighted imaging is directly associated with the movement of water, and thus the viability of tissue. For this reason it is assumed to be the a reliable golden standard in determining the infarct core volume within the first minutes after ictus[57–59].

The objective of this research is to implement automatic segmentation of the ADC infarct core based on Straka *et al.* [18]. Afterwards, a comparison with follow-up imaging must reveal whether this segmentation is reliable. It is expected that there exist a relation between the severity of the diffusion restriction and the acute infarct core volume.

3.1 Materials and methods

3.1.1 Patient selection

This study is a substudy of the MR CLEAN trial, which evaluates the safeness and effectiveness of intra-arterial treatment in patients with acute ischemic strokes. Patients were selected from the multi-center MR CLEAN database, and where admitted to the hospital between May 2012 and January 2014 suffering from an acute ischemic stroke. The inclusion and exclusion criteria of the MR CLEAN trial apply [60]. For this research, patients were selected who received a non-contrast CT and diffusion weighted imaging in the acute phase, as well as follow-up imaging 1 to 9 days after symptom onset.

3.1.2 Imaging protocol

Apparent diffusion coefficient

An ADC image is obtained from a diffusion weighted image (DWI). DWI is a balanced spin-echo echoplaner sequence acquired in the axial plane was obtained using the following parameter: TR 3444 to 6800 ms, TE 78 to 109 ms, b-value 1000 s/mm^2 and the matrix size was generally 128×128. In total, 19 patients in four different centers underwent diffusion weighted imaging in the acute phase. An overview of the scanner types and images resolution can be found in Table 3.1. A more detailed descripted of the acquisition and calculation of ADC value can be found in Sec. 2.1.

Table 3.1 Overview of the scanner types and the obtained image resolution sorted per institution.

Institution	Scanner	Resolution (mm)	n
1	Siemens Skyra 3T	1.198×1.198×4.95	1
2	Philips Intera 1.5 T	0.8984×0.8984×6	1
3	Siemens Avanto 1.5T	1.198×1.198×6.05	1
4	Siemens Avanto 1.5T	1.797×1.797×6.5	7
	Siemens Avanto 1.5T	1.797×1.797×5.2	7
	Philips Panorama 1T	1.438×1.438×6	2

Non-contrast CT

A non-contrast CT (NCCT) head CT scan was acquired with contiguous 5-mm thick axial slices at the admission of the hospital, with voxel sizes ranging from 0.41-0.59×0.41-0.59×5mm. An overview of the scanner types and settings is given in Table 3.2.

Table 3.2 Overview of the scanner types with the used reconstruction kernels and scanner settings.

Institution	Scanner	Kernel	mAs	kVp	n
1	Siemens SOMATOM Definition Flash	J45s\4	391	120	1
2	Toshiba Aquillon ONE	FL01	150	120	1
3	Toshiba Aquillon64	FC64	-	120	1
4	Philips Sensation 64	H31s	380	120	14
	Philips Sensation 64	H42s	380	120	1
	Philips Brilliance 40	UB	350	120	1

Follow-up imaging

Non-contrast computed tomography was used for follow-up. These images were obtained 1 to 9 days (median 5, Q1-Q3: 1-6.5) after symptom onset. In case of a craniectomy, the latest NCCT was obtained before the craniectomy. The voxel size lies between 0.35-0.59×0.35-0.59×3-5 mm. An overview of the used scanners, reconstruction kernels, and settings are listed in Table 3.3.

Table 3.3 Overview of the scanner types with the used reconstruction kernels and scanner settings.

Institution	Scanner	Kernel	mAs	kVp	n
1	Toshiba Aquillon	FC69	300	120	1
2	Toshiba Aquillon ONE	FL01	100	120	1
3	Philips iCT256	UB	490	100	1
4	Siemens Sensation 64	H31s	380	120	9
	Siemens Sensation 16	H31s	162	120	1
	GE Lightspeed16	Standard	396	120	1
	Siemens SOMATON Definition Flash	J40s\3	340	100	1
	Toshiba Aquillon ONE	FC22	300	135	1
	Toshiba Aquillon	FC22	190	120	1
	Philips Mx8000 IDT16	UB	350	120	1
	Philips Brilliance 40	UB	350	120	1

3.1.3 Registration

Multimodality registration

All registrations were performed by using the open-source software Elastix[61]. First the ADC was registered to baseline NCCT. As the skull contains minimal amounts of H_2O molecules, the skull is not visible on MR images. For this reason, we segmented the brain in the ADC image and NCCT using skull-stripping. Because of the alignment of multimodality images, mutual information (MI) was set as similarity measure. As there is a lack of direct relation between the intensity of the ADC and NCCT image, e.g. diffusivity vs. density, registration based on MI is maximizing the statistical dependence between both images [62,63]. Using the MI metric, a rigid transformation is performed, in which the major differences in position and orientation are corrected, followed by an affine transformation to correct for difference in positioning, rotation, scaling and shearing.

The baseline NCCT and the follow-up NCCT was registered using the sum of squared differences as similarity measure. In this case, only rigid transformation was performed.

Skull-stripping

Skull-stripping was based on a threshold operation; a threshold was set of 200×10^{-6} mm^2/s for the ADC value, and thresholds of -30 and 200 HU for the NCCT image. Afterwards 2D erosion was performed, followed by 2D connected component analysis. The largest connected component was chosen in one of the superior slices. If in the lower slices, more connected components were present, the one with the centroid closest to the superior slice was chosen. However, when multiple connected components could fit in the contour of the superior slice, these were all selected. After selecting the brain tissue, morphological dilation and closing operations were performed.

3.1.4 Midline detection

The midline is detected based on the bony structures of the NCCT. Using 2D principal component analysis for each slice, the average rotation of the axial slices is calculated (yaw) from the centroid of the image. The rotation in the coronal plane is also calculated (roll). An illustration of the different rotation axes of the head is given in Figure 3.1. Based on these two angles, a plane can be defined which separates the two hemispheres. It is possible to manually correct for the yaw angle, by placing a point on the falx cerebri.

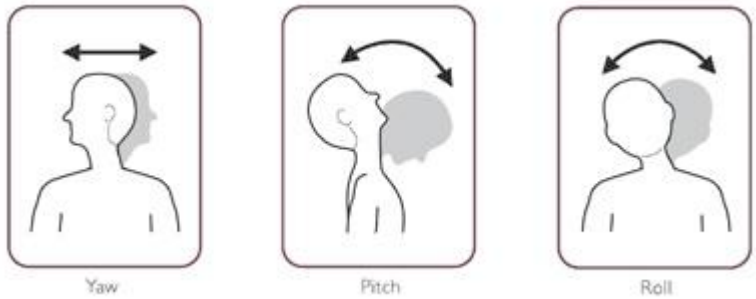

Figure 3.1 The three axis of rotation of the head

3.1.5 Segmentation of infarct core on ADC

As the infarct core is only present in one hemisphere, the midline was used to prevent the segmentation to leak into the other hemisphere. The segmentation of the infarct core is based on the threshold given in the article of Straka *et al.* [18]. Tissue with an apparent diffusion coefficient (ADC) below the 600×10^{-6} mm^2/s is identified as core. Morphological operations such as circular erosion and dilation were performed to reduce leaking of the infarct core towards other regions of the brain. Afterwards, the largest connected component was assumed to be infarct core. A small dilation was performed to get smooth edges of the infarct core, in case of a small core (under 5 mL), a 2D dilation of one pixel was performed, and otherwise the dilation was two pixels. Afterwards, the holes in the masked were filled. A hole is a set of background voxels which cannot be reached if the background is filled from the edge of the image.

Colormap of infarct core

A colormap of the severity of the diffusion restriction might be useful to visualize the differences in diffusion restriction within and between different cores. This colormap can be used as an overlay of the normal ADC image. Blue areas represent areas with no diffusion (0 $\times 10^{-6}$ mm^2/s), while red regions represent areas with a diffusion above 600 $\times 10^{-6}$ mm^2/s, as can be seen in Figure 3.2.

3.2 Results

An example of the midline detection and the segmentation of the image can be seen in Figure 3.3. The result of the colormap of the infarct core can be seen in Figure 3.2.

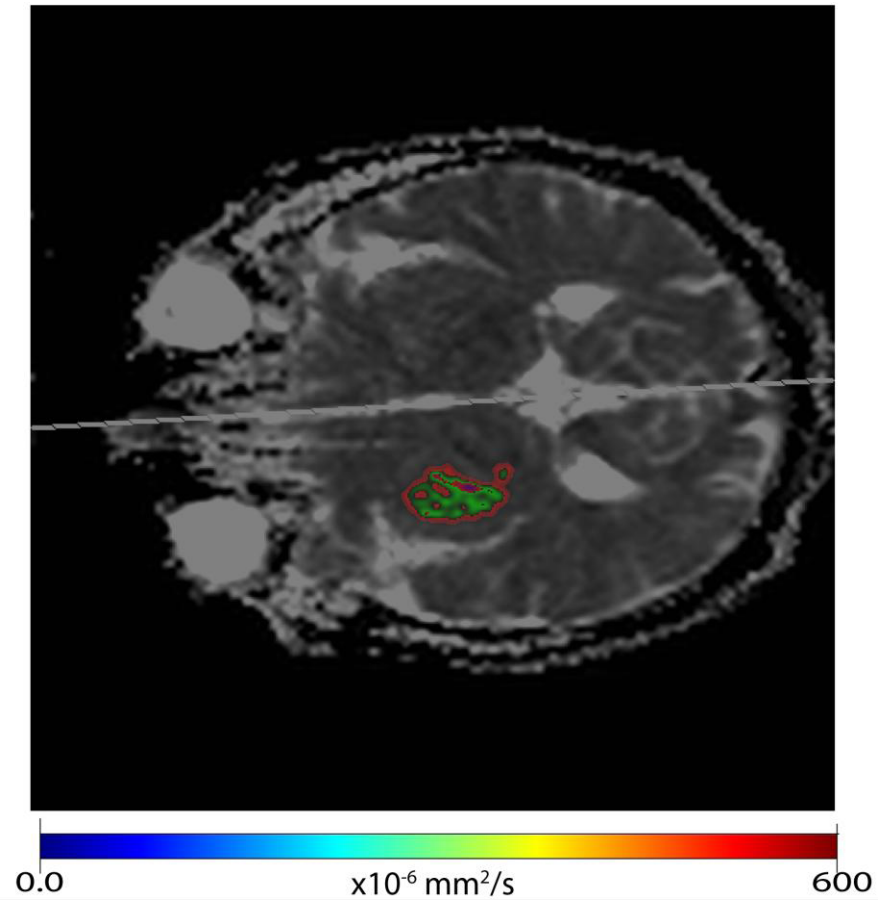

Figure 3.2 Result of the colormap of the infarct core

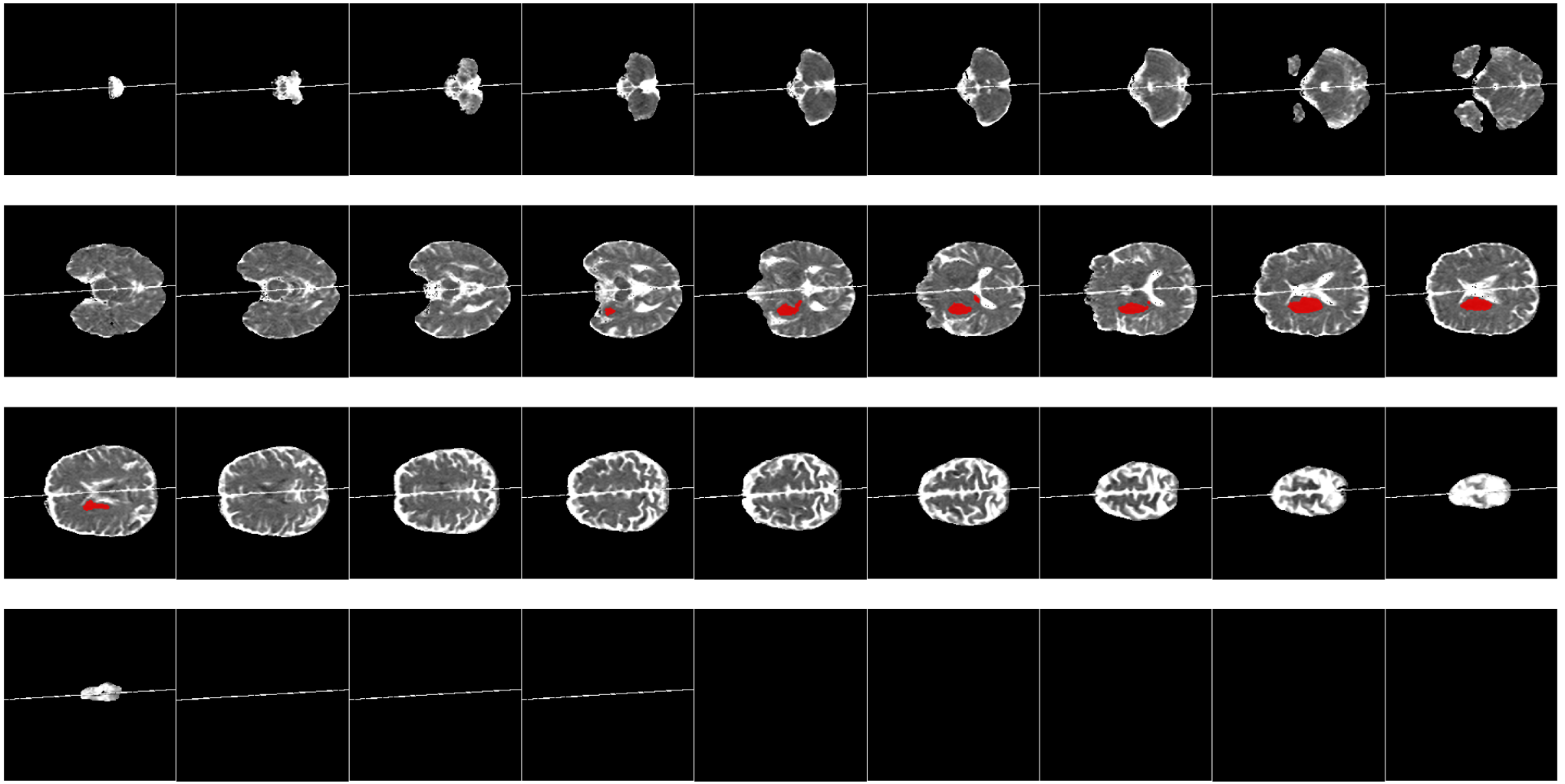

Figure 3.3 Result of skull-stripping, registration, the midline detection and segmentation of the infarct core.

The median infarct core size was 29.9 mL (Q1-Q3: 13.4-90.4 mL). The median diffusivity in the core was 465×10^{-6} mm^2/s (Q1-Q3: 371-549$\times10^{-6}$mm^2/s). The lowest median diffusivity in a patient was 394×10^{-6} mm^2/s, and was found in a fairly large infarct core of 95mL. In Figure 3.4 the median ADC values found in the core are plotted against the segmented infarct core volume. This data display a significant Pearson correlation (R^2=0.465, p<0.01).

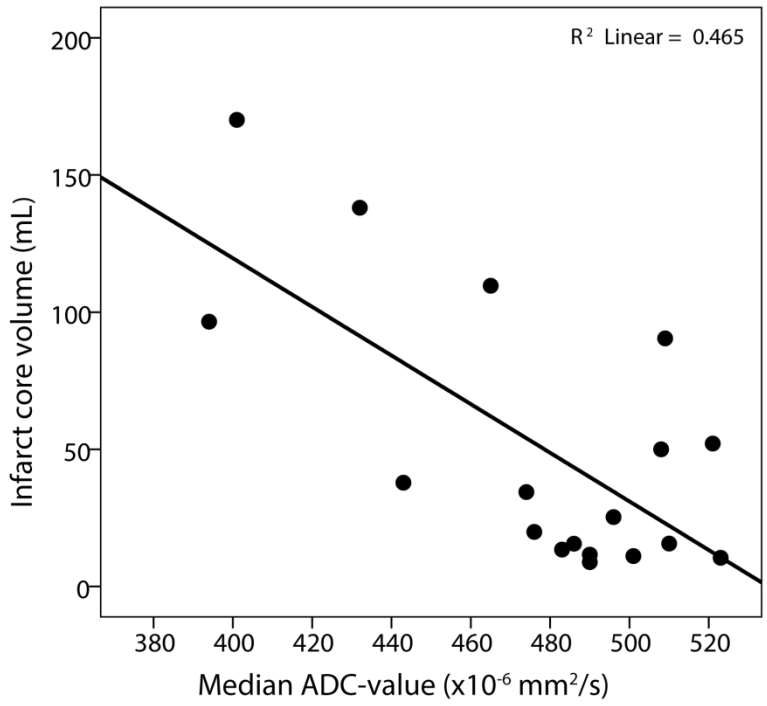

Figure 3.4 The median ADC-value plotted against the infarct core volume.

This observation supports the need of a colormap to indicate the severity of the diffusion restriction. Bigger infarct core volumes are associated with larger risks of hemorrhage [10,12,64], and thus lower ADC-values.

Qualitative comparison with the follow up data shows that the automatically segmented ADC core is located within the final infarct core for all patients. Three of the patients were excluded from this comparison due to the low image quality (i.e. motion artifacts, reconstruction) of the follow-up imaging.

3.3 Discussion

Automatic infarct core segmentation, based on apparent diffusion coefficient images, correctly predicted the location of the final infarct core in all patients. This finding suggests that ADC infarct core volume can be used as a reliable method to early determine the infarct core volume. Several articles mention that reversal of the DWI infarct core is rarely seen [57,65,66], and if seen, this would rarely effect the treatment decision making.

Thresholds used for the automatic segmentation of the infarct core were based on the findings of Straka *et al.* [18], which was designed for both 1.5T and 3.0T MRI scanners. However, Straka *et al.* notices in 10% of the patients severe motion, leading to artifacts and pleas for using better imaging techniques as well as more optimized imaging protocols [18].

Registration

Registration of the ADC image and NCCT image was optimized using the mutual intensity metric[62,63]. Although this metric is designed to do multimodality registration, still large registration errors can occur. To prevent major errors, skull-stripping was performed before registration. However, due to the large voxels in the ADC image, soft tissue of the brain was connected towards soft tissue in the nasal cavity. Although

substantial erosion was performed before the connected component analysis, this effect was difficult to avoid in all patients. Thereby is the registration hampered by the fact that in most cases, the volume of a single ADC-voxel was approximately 25× larger than that of the NCCT-voxel. This requires severe interpolation. The total registration takes around three minutes per patient. Afterwards, careful evaluation of the aligned images is needed, to check the alignment, as well as the image quality.

An addition to the current registration, a non-rigid registration with an atlas might be of additional value, i.e. for a better detection of the midline. In this research, the midline detection is based on 2D principal component analyses on the axial and coronal plane. In literature, a robust technique for midline detection was also described based on cross-correlation [67]. Implementation of this technique showed large errors, due to the thick skull in the back of the head. When using atlas-based midline detection, deformation of the midline can be included. Another advantage is that direct identification of the infarct region can be possible when for instance using one of the LONI Atlases [68] or automatic selection of the affected ASPECTS regions [69].

Treatment efficacy
The question about the infarct core volume initially arise from the lack of prove for the efficacy of IAT [10,14,15]. Nevertheless, the current insight is that IAT is effective in patients treated within a 6 h time interval [16]. For this reason, the question to select patients who are likely to benefit from IAT might be more widely applicable than initially thought. Currently, treatment decisions are mainly based on the time expired since the time of onset. However, the time of onset is not always clear, e.g. in wake-up strokes. In addition, it is known, that even after 12 to 24 hour after symptom onset, still viable penumbra can be present [70,71]. For these reasons, clinical decision making based on time alone is unlikely to provide the best selection criteria. Infarct core volume might be more predictive, as a large volume of the infarct core is associated with poor collateral flow [22,23]. It is known that the quality of the collateral flow is strongly associated with infarct growth [55,56]. The infarct core volume might be a new selection criterion for IAT. However, cut-off thresholds are present [14,72], more research could make these thresholds a little less arbitrary.

Future perspectives
Using diffusion weighted imaging for clinical decision making is preferred, nevertheless, it is not (yet) feasible in everyday clinical practice. This is due to the absence of a MRI scanner on the emergency department (ED), and thus limited availability. Apart from these logistics and time-consuming problems, not every patient is eligible for MR imaging, i.e. patients with metal implants such as pacemakers and joint replacements. Having a MRI scanner on the ED, combined with an exclusion of patients with metal implants would improve the clinical decision making.

3.4 Conclusion
Automatic segmentation of the infarct core on ADC images is possible using a threshold of 600×10^{-6} mm^2/s in combination with morphological operations. The median value of the diffusion restriction is associated with the infarct core size (R^2=0.47, $p<0.01$). Qualitative assessment of the ADC infarct core with the follow-up CT suggests no reversal of the ADC infarct core.

4. Image processing of perfusion computed tomography

Acute ischemic stroke (AIS) is the second cause of dead worldwide, and the leading cause of acquired disability in adults [1,4]. In AIS part of the brain is not sufficiently provided from blood flow due to a thrombus in the afferent vessel. All treatment options are based on the recanalization of the occluded vessel to restore the blood flow as soon as possible, and thus preventing the penumbra from infarction. Currently there are two main treatment options, namely (i) thrombolysis using recombinant tissue plasminogen activator intravenously (IV rtPA), which is proven to be beneficial within 4.5 hours after symptom onset and (ii) intra-arterial treatment (IAT), in which the thrombus can be mechanically removed from the vessel. Recently, it is proven that IAT within 6 hours after symptom onset is effective as an addition to the normal intravenous treatment [16]. A drawback of IAT is the higher risk of hemorrhage, certainly in large infarct cores [10,12,19], and thus better selection of patients, can further improve the efficiently of the IAT.

Currently, treatment decisions are mainly based on the time expired since the time of onset. However, the time of onset is not always clear, e.g. in wake-up strokes. In addition, it is known that even after 12 to 24 hour after symptom onset viable penumbra can still be present. For these reasons, clinical decision making based on time alone is unlikely to provide the best selection criterion. Infarct core volume might be more predictive, as a large volume of the infarct core is associated with poor collateral flow [22,23]. It is known that the quality of the collateral flow is strongly associated with infarct growth[55,56]. Moreover, hemorrhages are more common in large infarct cores [64], and for this reason the selection based on infarct core volume might be twofold. In (i) patients with a good collateral flow, and therefore small infarct core outside the treatment window, a treatment might be beneficial, and (ii) in a patient with a poor collateral flow, and thus large infarct core, a better assessment can be made of the pros and cons, e.g. hemorrhage, of the IAT.

Diffusion weighted imaging (DWI) is assumed to be the a reliable golden standard in determining the infarct core volume within the first minutes after ictus[57,59]. However, this MR imaging is uncommon in Dutch emergency departments (ED), and not every patient is eligible for MR imaging, e.g.. patients with metal implants. Perfusion CT (CTP) is increasingly used as a diagnostic tool for patients suffering from acute ischemic stroke. It can be rapidly performed in almost every patient, and claims to be able to make a distinction between the infarct core and the salvageable penumbra [73,74].

It is known that using different commercial software on the same source data gives significant differences in the parameter maps [37]. Perfusion Mismatch Analyzer (PMA), designed by the Acute Stroke Imaging Standardization Group (ASIST-Japan) aims standardization of (CT) perfusion analysis in acute ischemic stroke [51]. Improving the post-processing of the source data, by implementing motion correction and TIPS bilateral filtering, is likely to improve the outcomes of PMA [53]. Afterwards, a comparison of the parameter maps obtained by various deconvolutions options, as offered by PMA, is done.

4.1 Materials and methods

4.1.1 Patient selection

This study is a substudy of the larger MR CLEAN trial, which evaluates the safeness and effectiveness of intra-arterial treatment in patients with acute ischemic strokes. Patients were selected from the multi-center MR CLEAN database, and where admitted to the hospital between May 2012 and January 2014 suffering from an acute ischemic stroke. The inclusion and exclusion criteria of the MR CLEAN trial apply [60]. For this research, patients were selected who received both a CTP and diffusion weighted imaging in the acute phase.

4.1.2 Imaging protocol

The CTP images were obtained using the following parameters: 80 kV and 150 mAs. Imaging at the level of the third ventricle was used, except for one patient, in which severe movement was observed during the CTP acquisition. For this patient, a CTP at the height of the second ventricle was used. For all 14 patients, the CTP consisted of 6 slices of each 4.8mm, and in total 25 time frames with a temporal resolution of two

seconds. An overview of the scanner types, as well as the voxel dimensions and reconstruction kernels is given in Table 4.1.

Table 4.1 Overview of the scanner types with the used reconstruction kernels and scanner settings.

Scanner	Kernel	Resolution (mm)	n
Siemens Sensation 64	B31s	0.5859×0.5859×4.8	12
Siemens Sensation 64	B31s	0.4648×0.4648×4.8	1
Siemens Sensation 64	B41f	0.4219×0.4219×4.8	1

4.1.3 Image processing

In the processing of perfusion CT data, the output is normally four different kinds of parameter maps. The cerebral blood volume (CBV) map, which is obtained by the area under the tissue attenuation curve or deconvolved, is normalized using the area under the curve of the arterial input function (AIF), as given by Formula 2.7. For the other maps, a delay (in)sensitive singular value decomposition (SVD) is used. More detailed information about obtaining these parameter maps using SVD is given in Sec. 2.1.4. The MTT map is obtained by the integral of the residue function (R(t)), which is the output of the SVD. A simple calculation gives the cerebral blood flow (CBF), which is $CBF = CBV/MTT$. The last frequently used parameter map is the Tmax, which is defined as the time to the maximum of the residue function.

There are different options of singular value decomposition in the Perfusion Mismatch Analyzer (PMA). The three options most commonly used are standard SVD (sSVD), block-circulant SVD (bSVD) and delay-corrected SVD based on arrival time (dSVD(AT)). Kudo *et al*. concluded that bSVD gives the most reliable results in case of tracer delay [37,45,75]. To optimize the results of PMA, a few pre-processing steps were taken.

4.1.3.1 Pre-processing

Motion correction

The different time frames of the raw CTP were sorted using MeVisLab [76]. Afterwards, all the time frames were registered to the first time frame using rigid and affine registration based on minimizing the sum of squared differences between the time frames.

TIPS filter

After the registration of the several time frames towards the first time frame, the data was filtered using a TIPS filter, as described in Section 2.3.2.1. To reduce the variance between patients, the profile-similarity SD (σ_ζ) was set constant on 250 (arb.units). The standard deviation (σ_d) was set to 9 mm. The total kernel size was restricted towards a 2D kernel of 15 by 15 pixels (≈7.5 × 7.5 mm) due to computational time limitations. Filtering took approximately 10-15 minutes per patient.

4.1.3.2 Processing in PMA

The processing of the pre-processed CTP data was performed by PMA in the automatic mode using one deconvolution. First the image was motion corrected and some noise reduction was performed. To this end, the Gaussian filter was removed from the original workflow. Afterwards some basic maps, like the CBV map (based on area under the curve) were calculated. Afterwards the arterial input function (AIF) and venous output function (VOF) were selected.

AIF selection

The arterial input function (AIF) is obtained from several points placed in the region of the internal carotid artery (ICA) to the M2 segment of the middle cerebral artery (MCA). PMA automatically places these points; however, manual adjustments are frequently necessary.

VOF selection
The location of the venous output function (VOF) was placed automatically in the superior sagittal sinus. Although PMA claims to automatically detect this sinus, manual adjustments were regularly needed.

Finally, a choice can be made to select a technique for the singular value decomposition, as described in detail in Section 2.3.1 to obtain other parameter maps. All these maps can be exported as an Analyze file.

4.2 Results

TIPS filtering of the motion-corrected CTP data reduces the noise, while the image still contains the sharp edges, as expected in case of bilateral filtering. In Figure 4.1, an optical comparison of the original data and the filtered data, and the tissue curves, can be made.

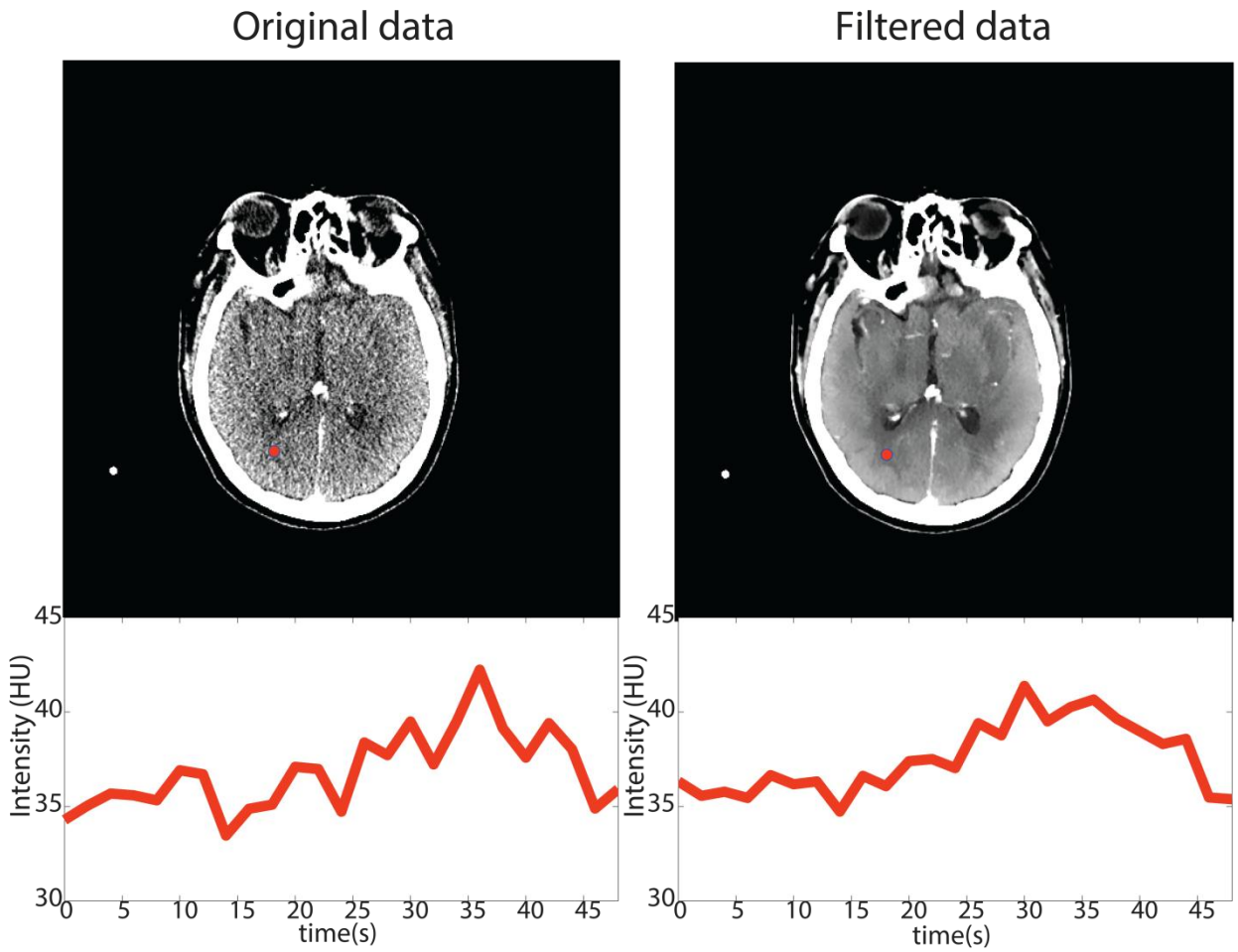

Figure 4.1 Optical comparison of the original data and the TIPS filtered data and the corresponding tissue curves.

Comparison of the CTP parameter maps gives large differences between the various SVD-techniques. An overview of the different deconvolutions and the differences is shown in Figure 4.2.

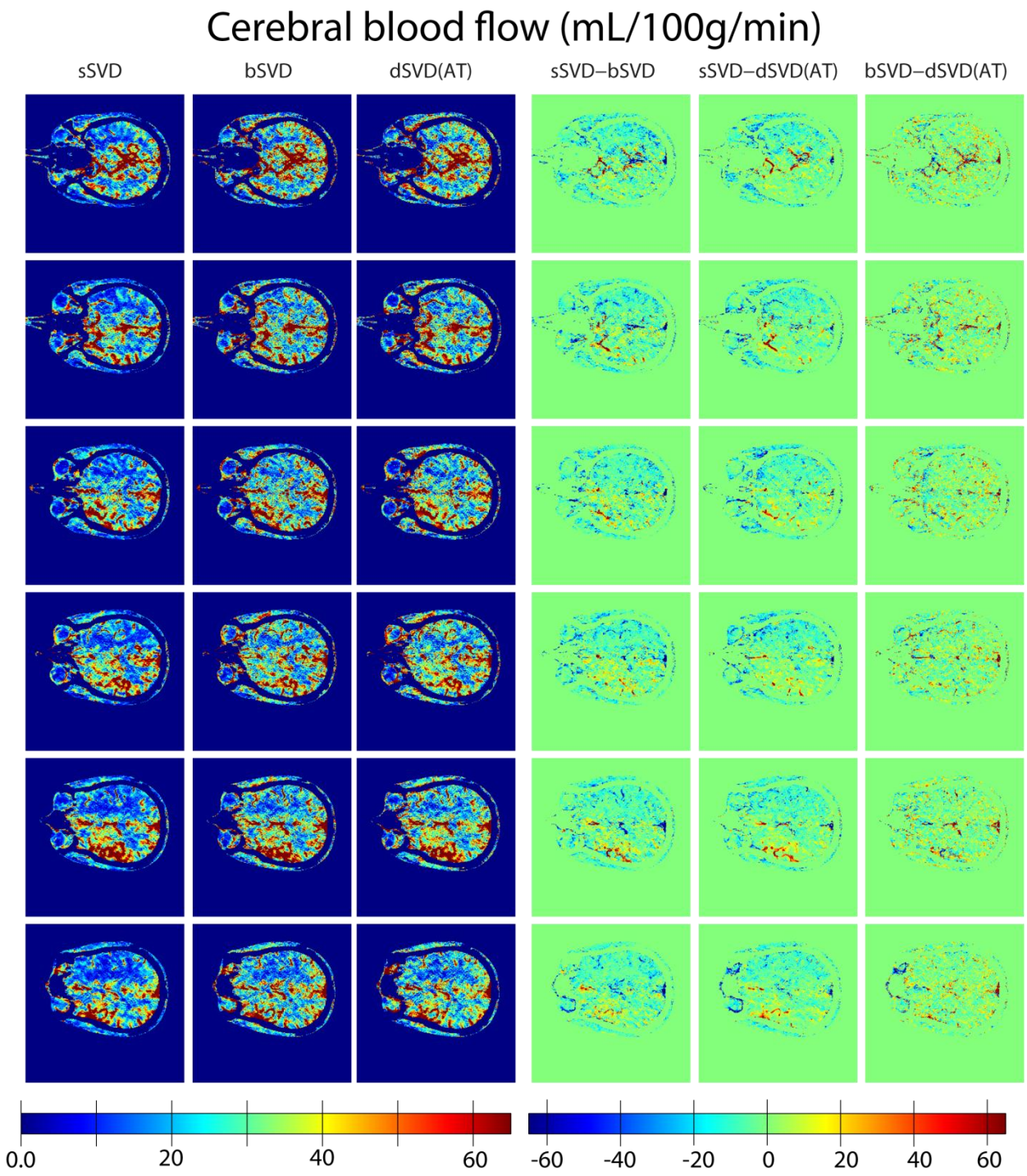

Figure 4.2 The CBF parameter maps of the used SVD-techniques on the left, and these maps on the right, in which blue is a maximal negative difference, green is no difference and red is a maximal positive difference.

The largest differences between the SVDs are observed around the large vessels. However, outside the vessels, differences are also observed. Differences for MTT and Tmax were even larger than the differences seen in the CBF. In Figure 4.4, the differences between the deconvolution of the fourth slice can be seen for both MTT and Tmax.

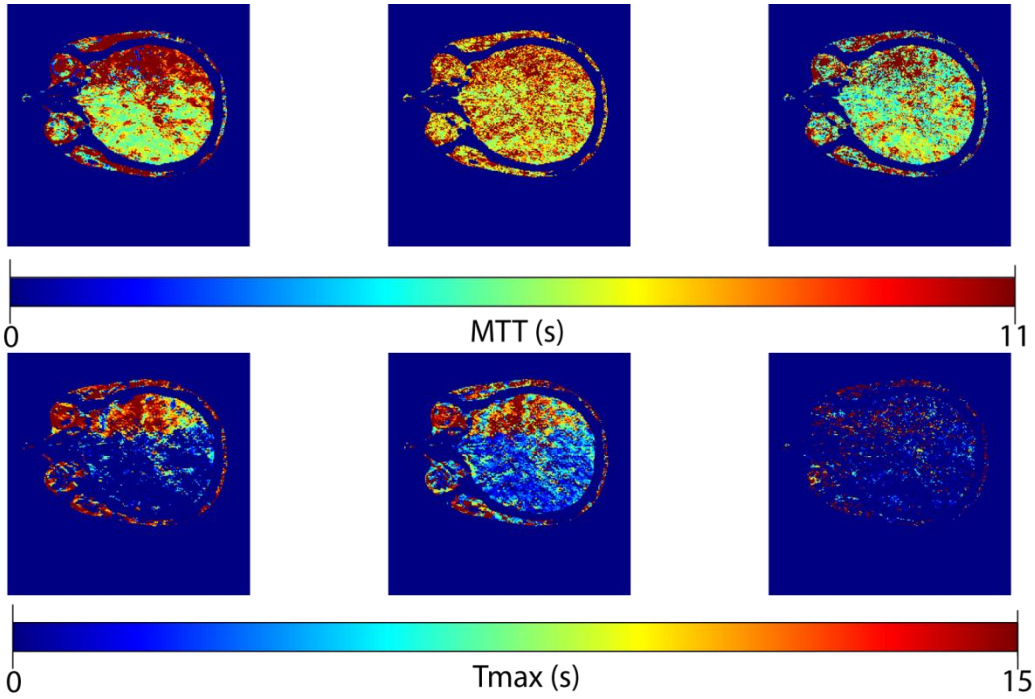

Figure 4.2 Optical comparison of the different SVD-techniques for both MTT and Tmax.

4.3 Discussion

Singular value decomposition

Using singular value decomposition for the analysis of perfusion of the brain is prone to errors. It is known that using different commercial software on the same datasets gives significant differences [37]. This is assumed to be caused by the differences in tracer-delay sensitivity. However, in our two delay insensitive methods (bSVD and dSVD(AT)), large differences can still occur, certainly in the MTT and Tmax maps. Recently, many articles about CTP used bSVD provided by PMA as golden standard [17].

It is also known that in case of severe hypoperfusion, a negative Tmax can be calculated, and is therefore not always reliable [46,75]. Kudo *et al.* concludes that the Tmax value of bSVD was the most reliable one, but also concludes that the Tmax parameter is highly dependent on tracer delay, as well as deconvolution technique [75]. PMA offers a SVD technique correcting for the Tmax, and due to the dependency of the Tmax on both tracer delay as well as deconvolution technique, we decided to take it aside. In most articles published by the ASIST Group, this type SVD is also not mentioned.

It is assumed that SVD is more robust than for instance the maximum slope model, i.e. by tracer delay. For this reason, most commercial software packages use SVDs nowadays. A novel option is the model dependent Bayesian hemodynamic parameter estimation, as offered by the OLEA software [46], a more detailed explanation can be found in Sec. 2.3.1. This estimation is described to be more stable, and the correlation between the real and observed perfusion is superior compared to SVDs [47,48]. Nevertheless, this Bayesian estimation is proven to be beneficial if the signal to noise ratio (SNR) is above 5, however an SNR of 10 and higher is preferred.

Motion correction

The motion correcting is based on the registration of every timeframe towards the first obtained time-frame of the CTP. This kind of registration is different from the registration used in the research of Fahmi *et al* [76]. Due to the limited coverage of the CTP, it was preferred to register towards the first time frame, to reduce the loss of voxels.

TIPS filter

The current CTP acquisition is limited to a volume of approximately 30 mm. The SNR is low, and thus severe filtering of the data is needed. The largest advantage of using a TIPS bilateral filter is no reduction of the amplitude of the tissue attenuation curves. Gaussian filtering is expected to reduce this amplitude. Due to the time consuming operations of the TIPS bilateral filter, the size of the kernel was restricted. In optimal filtering, the kernel size is up to three times the standard deviation (σ_d), meaning that in our research kernels of approximately 55 pixels could be used. This would make the calculation around 13x as slow. The filtering in the z-direction would increase the filtering time also drastically; for those reasons an optical trade-off between time and optimal filter settings was made.

PMA

PMA uses, in contradiction to some commercial software, no vessel mask. The use of a vessel mask would decrease the number of extreme values in the parameters mask.

CTP acquisition

Length of the acquisition is 25 intervals over a period of 48 seconds. Current guidelines advise an acquisition time of at least 70 seconds [57,7777]. Another progress to reduce the radiation dose is the introduction of variable time intervals during the acquisition. This gives the opportunity to scan frequently during periods when large changes in the tissue attenuation curves are expected. Less frequent acquisition is possible in i.e. the end of the acquisition.

4.4 Conclusion

The post-processing of CTP has been extended by using motion correcting and TIPS bilateral filtering. PMA is used for obtaining the parameter maps. Large differences between the different deconvolutions are observed, mainly in the MTT and the Tmax.

5. Comparison of the infarct cores

Acute ischemic stroke (AIS) is the second cause of dead worldwide, and the leading cause of acquired disability in adults [1,4]. In AIS part of the brain is not sufficiently provided from blood flow due to a thrombus in the afferent vessel. All treatment options are based on the recanalization of the occluded vessel to restore the blood flow as soon as possible, and thus preventing the penumbra from infarction. Currently there are two main treatment options, namely (i) thrombolysis using recombinant tissue plasminogen activator intravenously (IV rtPA), which is proven to be beneficial within 4.5 hours after symptom onset [9] and (ii) intra-arterial treatment (IAT), in which the thrombus can be mechanically removed from the vessel. Recently, it is proven that IAT within 6 hours after symptom onset is effective as an addition to the normal intravenous treatment [16]. A drawback of IAT is the higher risk of hemorrhage, certainly in large infarct cores [10,12,19], and thus better selection of patients, can further improve the efficiently of the IAT.

Currently, treatment decisions are mainly based on the time expired since the time of onset. However, the time of onset is not always clear, e.g. in wake-up strokes. In addition, it is known that even after 12 to 24 hour after symptom onset viable penumbra can still be present. For these reasons, clinical decision making based on time alone is unlikely to provide the best selection criterion. Infarct core volume might be more predictive, as a large volume of the infarct core is associated with poor collateral flow [22,23]. It is known that the quality of the collateral flow is strongly associated with infarct growth[55,56]. Moreover, hemorrhages are more common in large infarct cores, and for this reason the selection based on infarct core volume might be twofold. In (i) patients with a good collateral flow, and therefore small infarct core outside the treatment window, a treatment might be beneficial [17], and (ii) in a patient with a poor collateral flow, and thus large infarct core, a better assessment can be made of the pros and cons, e.g. hemorrhage, of the IAT.

Diffusion weighted imaging (DWI), and its derivate apparent diffusion coefficient (ADC) image, is assumed to be the a reliable golden standard in determining the infarct core volume within the first minutes after ictus[57,59]. However, this MR imaging is uncommon in Dutch emergency departments (ED). Perfusion CT (CTP) is increasingly used as a diagnostic tool for patients suffering from acute ischemic stroke. It can be rapidly performed in almost every patient, and claims to be able to make a distinction between the infarct core and the salvageable penumbra [73].

Segmentation of the infarct core on CTP using the Philips workstation can give a false positive core (meaning that this part of the CTP core is not in the final infarct region) up to 60% of the CTP infarct core [78]. This implies that the current segmentation of the infarct core on CTP is not optimal and raises the question whether it is possible to optimize the CTP data analysis based on the segmented ADC infarct core, using analysis of the absolute and relative parameter values found in the infarct core, as well as applying a combination of thresholds using voxel-based machine learning.

5.1 Materials and methods

5.1.1 Patient selection

This study is a substudy of the larger MR CLEAN trial, which evaluates the safeness and effectiveness of intra-arterial treatment in patients with acute ischemic strokes. Patients were selected from the multi-center MR CLEAN database, and where admitted to the hospital between May 2012 and January 2014 suffering from an acute ischemic stroke. The inclusion and exclusion criteria of the MR CLEAN trial apply [60]. We selected patients who received a non-contrast CT, CTP and diffusion weighted imaging in the acute phase, as well as follow-up imaging 1 to 9 days after symptom onset.

5.1.2 Imaging protocol

CT perfusion

The CTP images were obtained using the following parameters: 80 kV and 150 mAs. Imaging at the level of the third ventricle was used, except for one patient, in which severe movement was observed during the CTP acquisition. For this patient, a CTP at the height of the second ventricle is used. For all patients, the CTP consisted of six slices of each 4.8mm, and in total 25 time frames with a temporal resolution of two seconds. An overview of the scanner types, as well as the voxel dimensions and reconstruction kernels is given in Table 5.1.

Table 5.1 Overview of the scanner types with the used reconstruction kernels and scanner settings.

Scanner	Kernel	Resolution (mm)	n
Siemens Sensation 64	B31s	0.5859×0.5859×4.8	12
Siemens Sensation 64	B31s	0.4648×0.4648×4.8	1
Siemens Sensation 64	B41f	0.4219×0.4219×4.8	1

Apparent diffusion coefficient

The ADC image is obtained from the diffusion weighted image (DWI). The median time between the acquisition of the CTP and DWI was 65.5 minutes (Q1-Q3: 54-79 m). This balanced spin-echo echoplaner sequence acquired in the axial plane was obtained using the following parameter: TR 3444 to 5134 ms, TE 89 to 109 ms, b-value 1000 s/mm2 and the matrix size was 128×128. In total, 14 patients underwent diffusion weighted imaging in the acute phase, an overview of the scanner types and images resolution can be found in Table 5.2.

Table 5.2 Overview of the scanner types and the obtained image resolution.

Scanner	Resolution (mm)	n
Siemens Avanto 1.5T	1.797×1.797×6.5	6
Siemens Avanto 1.5T	1.797×1.797×5.2	6
Philips Panorama 1T	1.438×1.438×6	2

Non-contrast CT

A non-contrast CT (NCCT) head CT scan was acquired with contiguous 5-mm thick axial slices at the admission of the hospital. An overview of the scanner types and setting and reconstruction kernels is given in Table 5.3.

Table 5.3 Overview of the scanner types with the used reconstruction kernels and scanner settings.

Scanner	Kernel	mAs	kVp	n
Philips Sensation 64	H31s	380	120	12
Philips Sensation 64	H42s	380	120	1
Philips Brilliance 40	UB	350	120	1

Follow-up imaging

Non-contrast computed tomography was used for follow-up. These images were obtained 1 to 9 days (median 3, Q1-Q3: 1-6.25) after symptom onset. In case of a craniectomy, the latest NCCT was obtained before the craniectomy. The voxel size lies between 0.35-0.59×0.35-0.59×3-5 mm^3. An overview of the used scanners, reconstruction kernels, and settings are listed in Table 5.4.

5.1.3 Registration

Registration of the different image modalities is done as described in Sec. 3.1.3. and 4.1.3.1. Afterwards the CTP images are registered towards the NCCT using rigid and affine registration in Elastix [61], using the sum of

squared differences metric. Afterwards, the parameters maps were sorted and transformed, using Transformix, towards the baseline NCCT.

Table 5.4 Overview of the scanner types with the used reconstruction kernels and scanner settings.

Scanner	Kernel	mAs	kVp	n
Siemens Sensation 64	H31s	380	120	8
GE Lightspeed16	Standard	396	120	1
Siemens SOMATON Definition Flash	J40s\3	340	100	1
Toshiba Aquillon ONE	FC22	300	135	1
Toshiba Aquillon	FC22	190	120	1
Philips Mx8000 IDT16	UB	350	120	1
Philips Brilliance 40	UB	350	120	1

5.1.4 Gray matter mask

As the physiological function between gray and white matter is different, a difference in perfusion parameters is expected and has also been observed in several studies [30,31,36]. After some simple thresholding of the ADC image, based on the threshold inspired by Arakawa *et al.* [30], k-means clustering is conducted. K-means clustering partitions all the voxels in k-clusters, based on the nearest mean. After applying a threshold to the image, areas with a perfusion of more than 870×10^{-6} mm^2/s is identified as gray matter, while areas with perfusion between 600×10^{-6} mm^2/s and 870×10^{-6} mm^2/s are identified as white matter. A simple location weighted k-means clustering algorithm can divide the three different groups, i.e. the air, the gray and the white matter. Afterwards, the cluster with the highest percentage of values in between 870×10^{-6} mm^2/s and 1300×10^{-6} mm^2/s is selected to be gray matter and the holes are filled. To make sure that gray matter is also detected in the region of the ventricles and close to the skull, were cerebrospinal fluid (CSF) is present; a threshold of 1300×10^{-6} mm^2/s is applied on the ADC image, and afterwards again location weighted k-means clustering. This CSF mask is again selected and added to the existing segmentation of the gray matter, followed by filling the mask to remove gaps between the gray matter and CSF segmentation. Afterwards, small 2D radial erosion is applied on the CSF mask, and subtracted from the filled gray matter mask.

5.1.5 Calculation of perfusion parameters

In the calculation of the average perfusion in the core and in the healthy contralateral hemisphere, a distinction has been made between the gray and the white matter, based on the gray matter mask.

Statistical analysis

The values inside the infarct core, and in the contralateral hemisphere, are analyzed using the Statistics Toolbox of MATLAB. First, the data is tested whether it is normally distributed using a Kolmogorov-Smirnov test. In case of a normal distribution an unpaired two-sample-t-test is performed subsequently, otherwise a Mann Whitney U test. A Kruskal-Wallis test is done to test whether more than two groups are statistically different.

5.1.6 Relative comparison with contralateral hemisphere

As current segmentation of the infarct core is mostly based on the use of relative thresholds, a similar comparison is also done in this research. As the midline is calculated as in Section 3.1.4, the brain can be mirrored over this midline. Firstly, the center of gravity of the brain is moved towards the center of the image. Afterwards, the image is rotated to correct for the roll angle. In this case, due to small coverage of the CTP data (~3cm), patients with significant yaw angle were excluded, as there is a lack of a healthy contralateral side. In total, six patients were eligible for the comparison with the contralateral side. A vessel mask, a threshold of 130 HU is applied on the maximum intensity projection of the complete CTP series, was applied to avoid the influence of vessels in the core region. A circular 2D filter with a radius of three voxels was applied to reduce the noise in the image.

Statistical analysis

The relative values inside the infarct core were analyzed using the Statistics Toolbox of MATLAB. First, the distribution of the relative intensities was tested whether normally distributed using a Kolmogorov-Smirnov test. A two-sided one-sample t-test (in case of normal distribution) or a sign test was performed for the different parameter maps to test whether the relative values in the core were deviate from unity. The relative values in the infarct core are also compared with the relative values in the remainder of the affected hemisphere. In case of a normal distribution in both regions, an unpaired two-sample t-test is performed, otherwise a Mann Whitney U test.

Voxel-based machine learning

Using the Statistics toolbox in MATLAB, voxel based supervised learning is performed. Supervised learning uses a combination of thresholds, in a certain order, to obtain the best possible results. Both relative as absolute values per deconvolution are used as input, the segmentation of the ADC image is set as golden standard. Using classification trees, naïve Bayesian classification as well as support vector machines, the dataset is trained using the leave-one-patient-out method. Afterwards the excluded patient was analyzed using the outcomes of these classifications methods. Naïve Bayes performs poor for large datasets, and for this reason, we excluded this way of supervised learning. Support vector machines (SVMs) can have a high accuracy, but are computational demanding. Classification trees have a reasonable accuracy and are fast compared to SVMs.

5.2 Results

Perfusion parameters in infarct core

There are significant differences between the parameter values found in healthy gray matter (GM) and white matter (WM) for sSVD, bSVD and dSVD(AT). The median values, first and third quartile for healthy white and gray matter can be found in Table 5.5.

Table 5.5 The found median values (and the first and third quartile) of the various parameter maps per SVD-technique. A distinction can be made between white and gray matter in both healthy and core tissue.

		sSVD		**bSVD**		**dSVD(AT)**	
		Healthy	*Core*	*Healthy*	*Core*	*Healthy*	*Core*
CBF (mL/100g/min)	GM	29.1 (18.1-47.5)	21.9 (12.0-38.9)	*38.8 (25.0-58.0)*	27.8 (15.1-48.4)	33.9 (22.0-52.4)	27.5 (13.9-46.0)
	WM	22.2 (13.5-38.8)	15.5 (8.9-26.8)	*29.7 (18.3-47.6)*	20.8 (11.9-35.6)	26.8 (16.5-43.8)	20.0 (11.0-33.5)
CBV (mL/100g)	GM	2.1 (1.3-3.5)	1.5 (0.6-3.0)	2.5 (1.6-3.8)	1.9 (1.0-3.4)	2.2 (1.3-3.5)	1.7 (0.7-3.3)
	WM	1.5 (0.9-2.6)	1.0 (0.4-1.9)	1.9 (1.2-3.0)	1.4 (0.7-2.3)	1.6 (0.8-2.7)	1.1 (0.5-2.2)
MTT (s)	GM	9.2 (7.1-12.0)	9.1 (6.5-12.2)	7.9 (6.5-10.2)	8.3 (6.7-10.8)	8.1 (6.0-10.9)	7.9 (5.4-11.3)
	WM	8.6 (6.5-11.3)	8.6 (6.1-11.7)	7.8 (6.5-10.0)	8.0 (6.6-10.3)	7.3 (5.2-10.0)	7.5 (5.2-10.7)
Tmax (s)	GM	5.9 (2.2-10.4)	9.8 (5.1-15.0)	6.3 (3.4-12.4)	10.8 (5.6-17.4)	3.2 (1.0-7.4)	5.0 (1.5-11.9)
	WM	6.9 (2.7-12.3)	9.8 (4.9-15.1)	7.3 (3.8-14.2)	10.9 (5.5-17.6)	3.7 (1.1-10.2)	5.3 (1.4-12.7)

Using the Mann Whitney U test, significant differences were found between every parameter and SVD-technique between the healthy white matter and gray matter. Also significant differences between healthy tissue and core tissue were found for both gray matter as white matter.

The Kruskal-Wallis test gives us that all the groups are statistically different; however, a large overlap in the boxplots can be seen. The Kruskal-Wallis plots for the CBV and CBF parameter of all different SVD-techniques is shown in Figure 5.1.

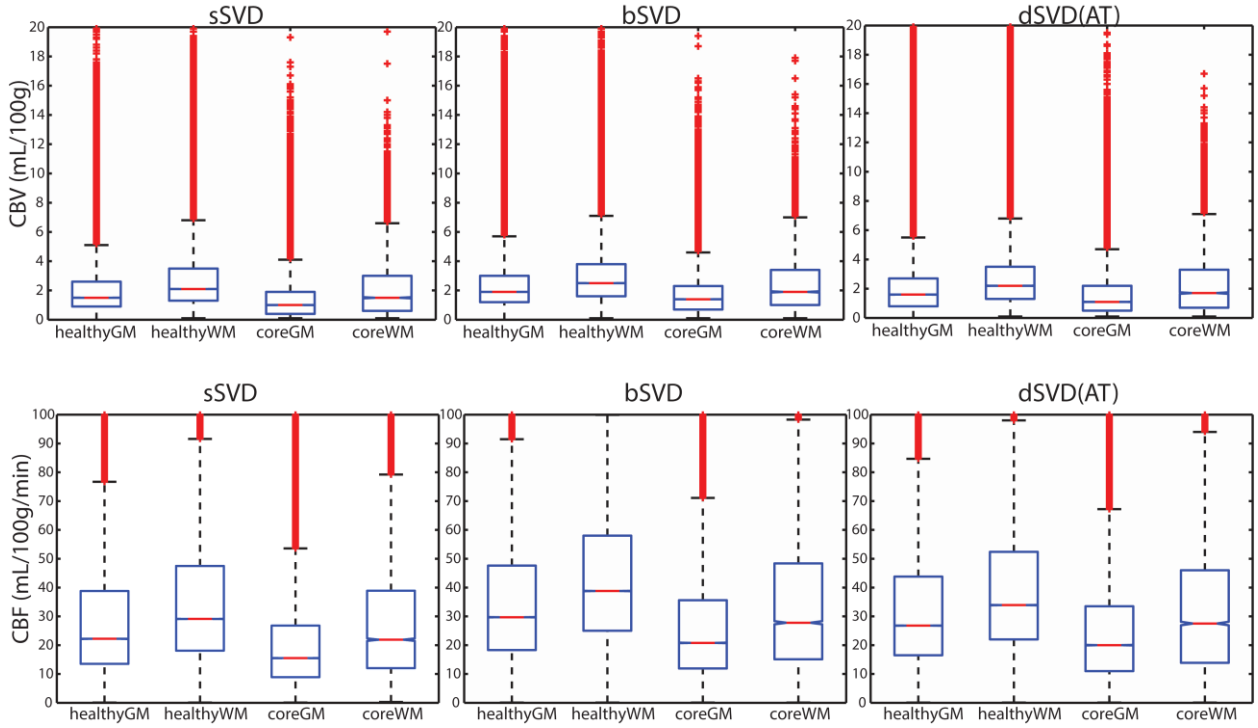

Figure 5.1 Kruskal-Wallis plots for CBV and CBF.

Relative comparison

The median values and the first and third quartiles for the different parameter maps in given in Table 5.6. The values in the core region of every patient differ significant from one (when the values in the contralateral hemisphere were equal to the core). A patient specific overview of the relative median value, first and third quartile, for the different SVD-techniques, differentiation between gray and white matter and parameter maps, can be found in Table 5.7. A patient specific overview of the relative median value, first and third quartile, for the different SVD-techniques, differentiation between gray and white matter and parameter maps, can be found in Table 5.7. Also a significant difference is found between the core values found in the gray matter and in the white matter.

Table 5.6 The found relative median values (and first and third quartile) for the various parameter maps and SVD-techniques.

Parameter	sSVD	bSVD	dSVD(AT)
CBF (mL/100g/min)	0.30 (0.17-0.54)	0.38 (0.23-0.65)	0.39 (0.22-0.66)
CBV (mL/100g)	0.31 (0.15-0.67)	0.39 (0.22-0.71)	0.42 (0.20-0.82)
MTT (s)	1.28 (0.91-1.73)	1.15 (0.94-1.40)	1.18 (0.90-1.54)
Tmax (s)	5.3 (1.4-23.8)	2.4 (0.7-5.4)	3.7 (1.0-13.5)

Significant differences between the core-region and the rest of the affected hemisphere were found in all six patients for almost all the different deconvolutions and parameter maps. If the patients were seen as a group, also significant differences were found.

Machine learning
The SVM often did not reach converged in the maximum number of iterations. Classification trees were analyzed, and a pruning of over 400 was regularly observed. This implicates that the classification of the combination of relative and absolute differences is not straightforward. The most observed relative threshold at the top was on basis of the relative CBV value of 0.5, the most observed absolute threshold was based on the difference in Tmax, however, this threshold showed a wide range.

5.3 Discussion

Time between acquisitions
The main caveat of this research is the elapsed time between the acquisition of the CT perfusion and the diffusion weighted imaging (DWI). The median time difference between these two acquisitions was 65 minutes. In this time frame, growth of the infarct core cannot be excluded. Saver *et al*. estimated the pace of neuronal loss, and indicates that in an hour around 120 million neurons are lost, 830 billion synapes and 714 km of myelinated fibers. This amounts to an aging of 3.6 years per hour [79]. However, the extent of the penumbral loss is not only based on time, but also on collateral flow and reperfusion [17]. For this reason, a one-to-one comparison of the ADC infarct core and the CT perfusion is not trivial. In this research, a one-to-one comparison is made. However, to correct partly for the infarct growth, the ADC infarct core in eroded with a 2D disk structuring element.

For this reason, perfusion parameters found for the ADC infarct core are not necessarily core only, but might also be part of the ischemic penumbra. To make sure that healthy tissue, used as a reference, is not part of the penumbra, we selected only voxels in the contralateral hemisphere to rule out any perfusion deficits in the reference tissue.

Comparison with recent research
The perfusion parameters found in this research are consistent with earlier findings [32,80]. For instance Philips is using a CBV<2.0 mL/100g, Campbell uses relative CBF value of 31% as a threshold [32]. Based on the medians and quartiles found in our patients, using the thresholds suggested by these articles, not the complete core could be segmented, and part of the healthy tissue will be included. Although we did find significant differences between the healthy tissue and the core (absolute and relative), segmentation is not possible using a fixed threshold for all patients. The found median values for the parameters for SVD technique varies widely per patient.

Relative threshold
From literature it is known that the relative thresholds are the most promising [32,35,81]. In this study, a relative comparison of hemisphere is not always possible due to the restricted brain coverage of the CTP images. In the six patients who were eligible for relative comparison, e.g. small yaw angle, significant differences between infarct core and rest of hemisphere in relative comparison. Nowadays, a 320-detector-row CT scanner is available, which is able to cover 16 cm of brain during the acquisition [82].

Table 5.7 Relative median and first and third quartile values for the different patients, for each parameter and two deconvolutions.

Patient	**1**		**2**		**3**		**4**		**5**		**6**	
	sSVD	**bSVD**	**sSVD**	**bSVD**	**sSVD**	**bSVD**	**sSVD**	**bSVD**	**sSVD**	**bSVD**	**sSVD**	**bSVD**
CBF (mL/100g/min)	0.38 (0.24-0.61)	0.55 (0.34-0.83)	0.30 (0.16-0.58)	0.37 (0.22-0.63)	0.47 (0.30-0.78)	0.54 (0.36-0.82)	0.49 (0.29-0.75)	0.47 (0.27-0.83)	0.19 (0.13-0.34)	0.28 (0.17-0.45)	0.49 (0.31-0.82)	0.63 (0.40-0.96)
WM	0.38 (0.25-0.59)	0.55 (0.36-0.81)	0.58 (0.34-0.81)	0.62 (0.40-0.89)	0.48 (0.31-0.77)	0.55 (0.37-0.80)	0.51 (0.33-0.76)	0.48 (0.29-0.85)	0.20 (0.13-0.33)	0.30 (0.20-0.46)	0.49 (0.28-0.78)	0.63 (0.36-0.90)
GM	0.27 (0.17-0.44)	0.41 (0.26-0.63)	0.22 (0.13-0.40)	0.30 (0.18-0.49)	0.37 (0.22-0.61)	0.44 (0.30-0.73)	0.40 (0.23-0.68)	0.40 (0.21-0.72)	0.17 (0.11-0.29)	0.25 (0.15-0.40)	0.76 (0.40-0.90)	0.94 (0.54-1.12)
CBV (mL/100g)	0.53 (0.29-0.90)	0.60 (0.38-0.92)	0.34 (0.17-0.72)	0.43 (0.25-0.75)	0.73 (0.43-1.13)	0.70 (0.44-1.06)	0.40 (0.20-0.81)	0.46 (0.26-0.87)	0.18 (0.10-0.33)	0.25 (0.15-0.42)	0.77 (0.44-1.08)	0.76 (0.48-1.05)
WM	0.53 (0.29-0.86)	0.60 (0.39-0.88)	0.62 (0.28-0.97)	0.73 (0.43-0.97)	0.75 (0.45-1.11)	0.71 (0.46-1.00)	0.42 (0.23-0.82)	0.48 (0.29-0.88)	0.17 (0.10-0.31)	0.26 (0.16-0.40)	0.71 (0.45-1.00)	0.73 (0.45-1.00)
GM	0.38 (0.21-0.69)	0.47 (0.30-0.73)	0.26 (0.14-0.50)	0.34 (0.21-0.58)	0.62 (0.37-1.11)	0.62 (0.38-1.06)	0.32 (0.15-0.75)	0.38 (0.21-0.78)	0.16 (0.09-0.29)	0.23 (0.14-0.38)	1 (0.54-1.21)	1 (0.62-1.16)
MTT (s)	1.53 (1.13-2.03)	1.20 (0.97-1.49)	1.29 (1.03-1.60)	1.21 (1.07-1.35)	1.44 (1.10-1.98)	1.31 (1.09-1.58)	1.00 (0.60-1.49)	1.06 (0.89-1.27)	1.22 (0.90-1.60)	1.12 (0.89-1.39)	1.43 (1.08-1.94)	1.17 (1.02-1.38)
WM	1.48 (1.11-1.94)	1.16 (0.95-1.42)	1.17 (0.94-1.42)	1.16 (1.02-1.28)	1.40 (1.09-1.86)	1.29 (1.08-1.54)	0.97 (0.60-1.44)	1.06 (0.90-1.25)	1.08 (0.81-1.39)	1.01 (0.82-1.22)	1.41 (1.10-1.82)	1.17 (1.04-1.35)
GM	1.77 (1.28-2.38)	1.34 (1.09-1.71)	1.32 (1.03-1.63)	1.23 (1.10-1.38)	1.85 (1.33-2.65)	1.49 (1.23-1.80)	1.04 (0.55-1.56)	1.07 (0.88-1.30)	1.27 (0.95-1.67)	1.19 (0.94-1.48)	1.33 (1.12-1.89)	1.05 (0.94-1.22)
Tmax (s)	11.9 (2.7-43.0)	3.5 (1.6-7.1)	3.9 (1.3-16.6)	2.3 (1.3-3.9)	2.9 (0.6-11.9)	3.0 (1.5-5.8)	2.5 (0.9-9.1)	2.0 (0.9-3.9)	11.0 (2.5-37.2)	1.5 (-1.8-5.3)	2.0 (0.0-13.0)	1.7 (0.6-4.8)
WM	12.9 (3.5-42.3)	3.2 (1.5-6.1)	2.1 (1.0-5.6)	1.7 (1.0-2.7)	2.9 (0.7-10.6)	3.1 (1.7-5.7)	2.8 (1.0-9.0)	1.8 (0.9-3.4)	8.5 (2.2-32.2)	1.2 (-1.6-4.1)	1.1 (-0.9-6.9)	1.6 (0.6-5.9)
GM	23.0 (3.2-67.5)	5.9 (2.8-12.1)	5.7 (1.7-23.5)	2.5 (1.4-4.5)	4.5 (1.0-22.9)	3.5 (1.6-7.1)	2.4 (0.8-9.5)	2.3 (0.9-4.6)	13.6 (2.6-42.4)	1.5 (-2.1-5.6)	2.0 (-3.0-11.9)	1.2 (0.5-2.9)

Atlas based registration
As already discussed in Sec. 3.3, atlas-based registration can improve the midline detection, as well as the location of the stroke. From the comparison of the perfusion parameters in the infarct core, it is proven that it is important to make a distinction between the gray and white matter. The segmentation of gray matter is constructed based on the ADC image. In the case of a diffusion restriction in both gray and white matter, the thresholding and k-means clustering, as described in Sec. 5.1.4, will not include all the gray matter. This results in an incorrect differentiation between gray and white matter in the core region, and therefore affects the median values found negatively. Using an atlas could prevent these problems, and further studies into the healthy perfusion of the different regions of the brain might also be of relevance for the determination of the correct thresholds. It is known that gray matter needs a higher blood flow to maintain vital, however, it is plausible that the basal ganglia would need even more blood flow. Another advantage of using atlas-based segmentation is that a better vessel mask can be applied. A vessel mask is applied during the relative comparison, based on a thresholded maximum intensity projection. However, the threshold is set high to prevent segmentation close to the skull. Regions close to the skull can have same intensities as the vessel, due to the partial volume effect. A probability map of the vessel, provided by the atlas, could improve the segmentation, and will lead to the use of a lower threshold.

We suspect that the effects of the lack of a vessel mask on the found medians and quartiles are marginal. However, if we analyze the boxplot of the Kruskal-Wallis test many outliers are observed, partly due to the lack of a vessel mask. The influence of vessels is present in both healthy and core tissue. Using a vessel mask in the absolute parameter comparison decreases the number of extremities, leading to slightly lower median values in the core tissue, as well as in the healthy reference tissue for both CBV and CBF. The median values of the MTT and Tmax might increase.

Machine learning
Voxel-based machine learning is not powerful enough to make an accurate distinction between core and healthy tissue. However, classification trees can give a rough indication of the most important thresholds, which are the ones at the basis of the tree. In contradiction to the research of Campbell *et al.* [32], the classification trees imply that the relative CBV is the most important parameter to make a distinction between healthy and core tissue.

5.4 Conclusion
Large overlap between the parameter values found in healthy and core tissue is observed. Differentiation between white and gray matter is essential in future research, as significant differences were found in the parameters in these tissues. Comparison with the contralateral side is most promising based on various classification trees.

References

1. Donnan GA, Fisher M, Macleod M, Davis SM, Royal S, Macleod UKM. Stroke. 2008;371.

2. Heuschmann PU, Di Carlo A, Bejot Y, et al. Incidence of stroke in Europe at the beginning of the 21st century. *Stroke.* 2009;40(5):1557–63.

3. Truelsen T, Piechowski-Jóźwiak B, Bonita R, Mathers C, Bogousslavsky J, Boysen G. Stroke incidence and prevalence in Europe: a review of available data. *Eur. J. Neurol.* 2006;13(6):581–98.

4. Mendis S. Stroke disability and rehabilitation of stroke: World Health Organization perspective. *Int. J. Stroke.* 2013;8(1):3–4.

5. Yoo AJ, Pulli B, Gonzalez RG. Imaging-based treatment selectiof for intravenous and intraarterial stroke therapies : a comprehensive review. *Expert Rev. Cardiovasc. Ther.* 2012;9(7):857–876.

6. Dirnagl U, Iadecola C, Moskowitz M a. Pathobiology of ischaemic stroke: an integrated view. *Trends Neurosci.* 1999;22(9):391–7.

7. Wardlaw JM. Neuroimaging in acute ischaemic stroke: insights into unanswered questions of pathophysiology. *J. Intern. Med.* 2010;267(2):172–90.

8. Goyal M, Menon BK, Derdeyn CP. Perfusion imaging in acute ischemic stroke: let us improve the science before changing clinical practice. *Radiology*. 2013;266(1):16–21.

9. Lansberg MG, Bluhmki E, Thijs VN. Efficacy and safety of tissue plasminogen activator 3 to 4.5 hours after acute ischemic stroke: a metaanalysis. *Stroke.* 2009;40(7):2438–41.

10. Broderick JP, Palesch YY, Demchuk AM, et al. Endovascular therapy after intravenous t-PA versus t-PA alone for stroke. *N. Engl. J. Med.* 2013;368(10):893–903.

11. Ruff J, Froehler MT. Status of endovascular interventions to treat acute ischemic stroke. *Curr. Treat. Options Neurol.* 2013;15(5):557–66.

12. Cloft HJ, Rabinstein A, Lanzino G, Kallmes DF. Intra-arterial stroke therapy: an assessment of demand and available work force. *AJNR. Am. J. Neuroradiol.* 2009;30(3):453–8.

13. Tomsick T, Broderick J, Carrozella J, et al. Revascularization results in the Interventional Management of Stroke II trial. *AJNR. Am. J. Neuroradiol.* 2008;29(3):582–7.

14. Kidwell CS, Jahan R, Gornbein J, et al. A trial of imaging selection and endovascular treatment for ischemic stroke. *N. Engl. J. Med.* 2013;368(10):914–23.

15. Lansberg MG, Straka M, Kemp S, et al. MRI profile and response to endovascular reperfusion after stroke (DEFUSE 2): a prospective cohort study. *Lancet Neurol.* 2012;11(10):860–7.

16. Berkhemer OA et al. Accepted for publication. 2014.

17. Jung S, Gilgen M, Slotboom J, et al. Factors that determine penumbral tissue loss in acute ischaemic stroke. *Brain.* 2013.

18. Straka M, Albers GW, Bammer R. Real-time diffusion-perfusion mismatch analysis in acute stroke. *J. Magn. Reson. Imaging.* 2010;32(5):1024–37.

19. Singer OC, Humpich MC, Fiehler J, et al. Risk for symptomatic intracerebral hemorrhage after thrombolysis assessed by diffusion-weighted magnetic resonance imaging. *Ann. Neurol.* 2008;63(1):52–60.

20. Hametner C, Ringleb PA, Hacke W, Kellert L. Selection of possible responders to thrombolytic therapy in acute ischemic stroke. *Ann. N. Y. Acad. Sci.* 2012;1268:120–6.

21. Yoo AJ, Verduzco L a, Schaefer PW, Hirsch J a, Rabinov JD, González RG. MRI-based selection for intra-arterial stroke therapy: value of pretreatment diffusion-weighted imaging lesion volume in selecting patients with acute stroke who will benefit from early recanalization. *Stroke.* 2009;40(6):2046–54.

22. Souza LCS, Yoo AJ, Kemmling A, Schaefer PW, Hirsch JA, Furie KL. Malignant CTA Collateral Profile is Highly Specific for Large Admission DWI Infarct Core and Poor Outcome in Acute Stroke. *AJNR. Am. J. Neuroradiol.* 2012;33(August 2012):1331–1336.

23. Morais LT, Leslie-Mazwi TM, Lev MH, Albers GW, Yoo AJ. Imaging-based selection for intra-arterial stroke therapies. *J. Neurointerv. Surg.* 2013;5(Supplement 1):i13–i20.

24. Barber PA, Demchuk AM, Zhang J, Buchan AM, Study A. Validity and reliability of a quantitative computed tomography score in predicting outcome of hyperacute stroke before thrombolytic therapy. *Lancet.* 2000;355:1670–1674.

25. Wardlaw JM, Orell M. Early Signs of Brain Infarction at CT : Observer Reliability and Outcome after Thrombolytic Treatment — Systematic Review 1. *Radiology.* 2005;(21):444–453.

26. Schellinger PD, Bryan RN, Caplan LR, et al. Evidence-based guideline: The role of diffusion and perfusion MRI for the diagnosis of acute ischemic stroke: report of the Therapeutics and Technology Assessment Subcommittee of the American Academy of Neurology. *Neurology.* 2010;75(2):177–85.

27. Schaefer PW, Grant PE, Gonzalez RG. Diffusion-weighted MR Imaging of the Brain. *Radiology.* 2000;(217):331–345.

28. Rana AK, Wardlaw JM, Armitage P a., Bastin ME. Apparent diffusion coefficient (ADC) measurements may be more reliable and reproducible than lesion volume on diffusion-weighted images from patients with acute ischaemic stroke–implications for study design. *Magn. Reson. Imaging.* 2003;21(6):617–624.

29. Purushotham A, Campbell BC V, Straka M, et al. Apparent diffusion coefficient threshold for delineation of ischemic core. *Int. J. Stroke.* 2013;(13):1–6.

30. Arakawa S, Wright PM, Koga M, et al. Ischemic thresholds for gray and white matter: a diffusion and perfusion magnetic resonance study. *Stroke.* 2006;37(5):1211–6.

31. Bristow MS, Simon JE, Brown R a, et al. MR perfusion and diffusion in acute ischemic stroke: human gray and white matter have different thresholds for infarction. *J. Cereb. Blood Flow Metab.* 2005;25(10):1280–7.

32. Campbell BC V, Christensen S, Levi CR, et al. Cerebral blood flow is the optimal CT perfusion parameter for assessing infarct core. *Stroke.* 2011;42(12):3435–40.

33. Campbell BC V, Christensen S, Levi CR, et al. Comparison of computed tomography perfusion and magnetic resonance imaging perfusion-diffusion mismatch in ischemic stroke. *Stroke.* 2012;43(10):2648–53.

34. Bivard A, Levi C, Spratt N, Parsons M. Perfusion CT in Acute Stroke : A Comprehensive Analysis of Infarct and. 2013;267(2):543–550.

35. Kamalian S, Kamalian S, Maas MB, et al. CT cerebral blood flow maps optimally correlate with admission diffusion-weighted imaging in acute stroke but thresholds vary by postprocessing platform. *Stroke*. 2011;42(7):1923–8.

36. Simon JE, Bristow MS, Lu H, et al. A novel method to derive separate gray and white matter cerebral blood flow measures from MR imaging of acute ischemic stroke patients. *J. Cereb. Blood Flow Metab.* 2005;25(9):1236–43.

37. Kudo K, Sasaki M, Yamada K, et al. Differences in CT Perfusion Maps Generated by Different Commercial Software : Quantitative Analysis by Using Identical Source Data of Acute Stroke Patient. *Radiology*. 2010;254(1).

38. Graessner J, Ing D. Frequently Asked Questions : Diffusion-Weighted Imaging (DWI). 2011:84–87.

39. Hagmann P, Jonasson L, Maeder P, Thiran J, Wedeen VJ, Meuli R. Understanding Diffusion MR Imaging Techniques : From Scalar Imaging to Diffusion. *RadioGraphics*. 2006;(26):205–224.

40. Bammer R. Basic principles of diffusion-weighted imaging. *Eur. J. Radiol.* 2003;45(3):169–84.

41. Ma L, Gao P-Y, Hu Q-M, et al. Prediction of infarct core and salvageable ischemic tissue volumes by analyzing apparent diffusion coefficient without intravenous contrast material. *Acad. Radiol.* 2010;17(12):1506–17.

42. Konstas a a, Goldmakher G V, Lee T-Y, Lev MH. Theoretic basis and technical implementations of CT perfusion in acute ischemic stroke, part 1: Theoretic basis. *AJNR. Am. J. Neuroradiol.* 2009;30(4):662–8.

43. Ostergaard L, Weisskoff RM, Chesler DA, Gyldensted C, Rosen BR. High Resolution Measurement of Cerebral Blood Flow using Intravascular Tracer Bolus Passages. Part I: Mathematical Approach and Statistical Analysis. *Magn. Reson. Med.* 1996;(36):715–725.

44. Wu O, Østergaard L, Weisskoff RM, Benner T, Rosen BR, Sorensen a G. Tracer arrival timing-insensitive technique for estimating flow in MR perfusion-weighted imaging using singular value decomposition with a block-circulant deconvolution matrix. *Magn. Reson. Med.* 2003;50(1):164–74.

45. Kudo K, Sasaki M, Ogasawara K, Terae S, Ehara S, Shirato H. Difference in Tracer Delay – induced Effect among Deconvolution Algorithms in CT Perfusion Analysis : Quantitative. 2009;251(1):241–249.

46. Boutelier T, Kudo K, Pautot F, Sasaki M. Bayesian Hemodynamic Parameter Estimation by Bolus Tracking Perfusion Weighted Imaging. 2012;31(7):1381–1395.

47. Sasaki M, Kudo K, Boutelier T, et al. Assessment of the accuracy of a Bayesian estimation algorithm for perfusion CT by using a digital phantom. *Neuroradiology*. 2013;55(10):1197–203.

48. Kudo K, Boutelier T, Pautot F, et al. Bayesian Analysis of Perfusion-weighted Imaging to Predict Infarct Volume: Comparison with Singular Value Decomposition. *Magn. Reson. Med. Sci.* 2014;13(1):45–50.

49. Wittsack HJ, Wohlschläger a M, Ritzl EK, et al. CT-perfusion imaging of the human brain: advanced deconvolution analysis using circulant singular value decomposition. *Comput. Med. Imaging Graph.* 2008;32(1):67–77.

50. Witkin AP. Scale-space filtering. 1987:1019–1022.

51. ASIST - Japan Acute Stroke Imaging Standardization Group. Available at: http://asist.umin.jp/index-e.htm.

52. Kosior JC, Kosior RK, Frayne R. Robust dynamic susceptibility contrast MR perfusion using 4D nonlinear noise filters. *J. Magn. Reson. Imaging.* 2007;26(6):1514–22.

53. Mendrik AM, Vonken E, van Ginneken B, et al. TIPS bilateral noise reduction in 4D CT perfusion scans produces high-quality cerebral blood flow maps. *Phys. Med. Biol.* 2011;56(13):3857–72.

54. Tomasi C, Manduchi R. Bilateral Filtering for Gray and Color Images. *Proceeding 1998 IEEE Int. Conf. Comput. Vis.* 1998.

55. Bandera E, Botteri M, Minelli C, Sutton A, Abrams KR, Latronico N. Cerebral blood flow threshold of ischemic penumbra and infarct core in acute ischemic stroke: a systematic review. *Stroke.* 2006;37(5):1334–9.

56. Campbell BC V, Christensen S, Tress BM, et al. Failure of collateral blood flow is associated with infarct growth in ischemic stroke. *J. Cereb. Blood Flow Metab.* 2013;33(8):1168–72.

57. Campbell BC V, Purushotham A, Christensen S, et al. The infarct core is well represented by the acute diffusion lesion: sustained reversal is infrequent. *J. Cereb. Blood Flow Metab.* 2012;32(1):50–6.

58. Bråtane BT, Bastan B, Fisher M, Bouley J, Henninger N. Ischemic lesion volume determination on diffusion weighted images vs. apparent diffusion coefficient maps. *Brain Res.* 2009;1279:182–8.

59. Merino JG, Warach S, Wood H. MEDSCAPE - Imaging of acute stroke. 2014:1–25. Available at: www.medscape.org.

60. Dippel DWJ, Roos YB, Majoie CBLM, Lugt A van der, Oostenbrugge R van, Zwam W van. MR CLEAN Trial protocol. 2014. Available at: www.mrclean-trial.org.

61. Klein S, Staring M, Murphy K, Viergever MA, Pluim JPW. elastix : A Toolbox for Intensity-Based Medical Image Registration. 2010;29(1):196–205.

62. Thévenaz P, Unser M. Optimization of Mutual Information for Multiresolution Image Registration. 2000;9(12):2083–2099.

63. Maes F, Vandermeulen D, Marchal G, Suetens P. Multimodality Image Registration by Maximization of Mutual Information. 1997;16(2):187–198.

64. Olivot J-M, Mosimann PJ, Labreuche J, et al. Impact of diffusion-weighted imaging lesion volume on the success of endovascular reperfusion therapy. *Stroke.* 2013;44(8):2205–11.

65. Chemmanam T, Campbell BC V, Christensen S, et al. Ischemic diffusion lesion reversal is uncommon and rarely alters perfusion-diffusion mismatch. *Neurology.* 2010;75(12):1040–7.

66. Olivot J-M, Mlynash M, Thijs VN, et al. Relationships Between Cerebral Perfusion and Reversibility of Acute Diffusion Lesions in DEFUSE Insights from RADAR. *Stroke.* 2009;40(5):1692–1697.

67. Liu Y, Collins RT, Rothfus WE. Robust Midsagittal Plane Extraction from Normal and Pathological 3-D Neuroradiology Images. 2001;20(3):175–192.

68. LONI Atlases. 2014. Available at: http://www.loni.usc.edu/atlases/.

69. Pexman JHW, Barber PA, Hill MD, et al. Use of the Alberta Stroke Program Early CT Score (ASPECTS) for Assessing CT Scans in Patients with Acute Stroke. *AJNR. Am. J. Neuroradiol.* 2001;117(September):1534–1542.

70. Furlan M, Marchal G, Viader F, Derlon J. Spontaneous Neurological Recovery after Stroke and the Fate of the Ischemic Penumbra. *Ann. Neurol.* 1996;40(2):216–226.

71. Marchal G, Beaudouin V, Rioux P, et al. Prolonged Persistence of Substantial Volumes of Potentially Viable Brain Tissue After Stroke : A Correlative PET-CT Study With Voxel-Based Data Analysis. *Stroke*. 1996;27(4):599–606.

72. Yoo AJ, Chaudhry Z a, Leslie-Mazwi TM, et al. Endovascular treatment of acute ischemic stroke: current indications. *Tech. Vasc. Interv. Radiol.* 2012;15(1):33–40.

73. Allmendinger AM, Tang ER, Lui YW, Spektor V. Imaging of stroke: Part 1, Perfusion CT--overview of imaging technique, interpretation pearls, and common pitfalls. *AJR. Am. J. Roentgenol.* 2012;198(1):52–62.

74. Biesbroek JM, Niesten JM, Dankbaar JW, et al. Diagnostic accuracy of CT perfusion imaging for detecting acute ischemic stroke: a systematic review and meta-analysis. *Cerebrovasc. Dis.* 2013;35(6):493–501.

75. Kudo K, Sasaki M, Østergaard L, et al. Susceptibility of Tmax to tracer delay on perfusion analysis: quantitative evaluation of various deconvolution algorithms using digital phantoms. *J. Cereb. Blood Flow Metab.* 2011;31(3):908–12.

76. Fahmi F, Marquering H a, Borst J, et al. 3D movement correction of CT brain perfusion image data of patients with acute ischemic stroke. *Neuroradiology*. 2014;56(6):445–52.

77. Kidwell CS, Jahan R, Gornbein J, et al. A Trial of Imaging Selection and Endovascular Treatment for Ischemic Stroke. *N. Engl. J. Med.* 2013;368(10):914–923.

78. Geuskens RREG. Private communication. 2014.

79. Saver JL. Time is brain--quantified. *Stroke*. 2006;37(1):263–6.

80. Abels B, Klotz E, Tomandl BF, Kloska SP, Lell MM. Perfusion CT in acute ischemic stroke: a qualitative and quantitative comparison of deconvolution and maximum slope approach. *AJNR. Am. J. Neuroradiol.* 2010;31(9):1690–8.

81. Schaefer PW, Barak ER, Kamalian S, et al. Quantitative assessment of core/penumbra mismatch in acute stroke: CT and MR perfusion imaging are strongly correlated when sufficient brain volume is imaged. *Stroke*. 2008;39(11):2986–92.

82. Diekmann S, Siebert E, Juran R, et al. Dose exposure of patients undergoing comprehensive stroke imaging by multidetector-row CT: comparison of 320-detector row and 64-detector row CT scanners. *AJNR. Am. J. Neuroradiol.* 2010;31(6):1003–9.